

Title

Montiel Abello

Acknowledgements

I would like to thank my supervisors...

Abstract

TEXT

Contents

Acknowledgments	i
Abstract	ii
1 Introduction	1
1.1 Literature Review	2
1.1.1 Infinite-Dimensional Observers	2
1.1.1.1 Linear Systems	2
1.1.1.2 Nonlinear Systems	3
1.1.2 Symmetry-Preserving Observers	4
1.1.2.1 Early work	4
1.1.2.2 Active Research	5
2 Theoretical Background	8
2.1 Rigid Body Kinematics	8
2.1.1 Lie Groups	8
2.1.1.1 Matrix Lie groups	9
2.1.1.2 Lie algebra	9
2.1.1.3 The exponential map and logarithm map	9
2.1.1.4 Infinitesimal generators	10
2.1.1.5 Lie bracket and group operation	11
2.1.1.6 Actions	11
2.1.2 $\text{SO}(3)$	11
2.1.2.1 Lie algebra	12
2.1.2.2 Actions	13
2.1.2.3 Rotation representations	13

2.1.2.4	Rotation matrices	13
2.1.2.5	Scaled-axis representation	13
2.1.2.6	Rotation quaternions	14
2.1.3	SE(3)	15
2.1.3.1	Lie algebra	15
2.1.3.2	Actions	16
2.1.4	Reference Frames	17
2.1.4.1	Pose	17
2.1.4.2	Point	18
2.1.4.3	Homogeneous coordinates	18
2.1.4.4	Redefining the reference frame of a point	18
2.1.4.5	Concatenating poses	19
2.1.4.6	Redefining the reference frame of a pose	19
2.1.4.7	Inverse	19
2.1.5	Rigid Body State Representation	19
2.1.6	Rigid Body Kinematics	20
2.1.7	Scanning Laser Rangefinder Dynamic Model	20
2.2	State Observers	22
3	Problem Statement	23
4	Simulation	27
4.1	Implementation	27
4.1.1	Rigid Body Motion	29
4.1.1.1	Interpolation	30
4.1.1.2	Numerical Integration	31
4.1.2	Sensor modelling: <code>initialisesensor</code>	32
4.1.2.1	Motion	32
4.1.2.2	Scanning	33
4.1.3	Environment Modelling: <code>initialiseenvironment</code>	34
4.1.3.1	Motion	34
4.1.3.2	Rigid Objects	35
4.1.4	Measurement Modelling	37
4.1.4.1	Range Computation: <code>computerange</code>	37

4.1.4.2	Sensor Noise: <code>addnoise</code>	38
4.1.5	Observer Implementation	40
4.1.5.1	Estimate: <code>estimatestate</code>	40
4.1.5.2	Object/background separation: <code>identifyobject</code>	40
4.1.5.3	Update: <code>updatestate</code>	41
4.2	Results	50
4.2.1	testing scheme? think of a title...	50
4.2.2	Orientation correction	50
4.2.3	Position correction	50
4.2.4	Size correction	60
4.2.5	Orientation and size	60
4.2.6	effect of initial conditions	65
4.2.7	discussion	65
5	Experiment	66
5.1	Sensor Noise Characterisation	67
5.1.1	Setup	67
5.1.2	Results	67
5.2	Testing Data Collection	72
5.2.1	Setup	72
5.2.2	Results	72
6	Conclusion	73

List of Figures

1.1	Infinite dimensional optical flow discretised and computed in separate, independent regions	7
2.1	Transformations between reference frames $\{F\}$, $\{A\}$ and $\{B\}$ defined with respect to $\{F\}$	17
3.1	caption	23
4.1	Scanning parameters	35
4.2	Cube modelled with ordered set of points and corresponding triangles	36
4.3	Ray-triangle intersection	37
4.4	Orientation update	43
4.5	Position update	45
4.6	Size update - case 1	48
4.7	Size update - case 2	49
4.8	Orientation correction - no noise	51
4.9	Orientation correction - noise	52
4.10	rotating - Orientation correction via screw - no noise	53
4.11	rotating - Orientation correction via twist - no noise	54
4.12	rotating - Orientation correction via screw - noise	55
4.13	rotating - Orientation correction via twist - noise	56
4.14	stationary, 1 face visible - position correction	57
4.15	stationary with noise, 1 face visible - position correction	58
4.16	stationary with noise, 2 faces visible - position correction doesn't work	59
4.17	stationary with noise, 3 faces visible - size correction	60
4.18	rotating + translating with noise, 3 faces visible - size correction	61

4.19 stationary with noise, 3 faces visible - orientation and size correction	62
4.20 rotating with no noise, 3 faces visible - orientation (via screw) and size correction	63
4.21 rotating with no noise, 3 faces visible - orientation (via twist) and size correction	64
4.22 Tetrahedron: orientation & size correction	65
5.1 $r_{error}(r, \theta)$ approximately normally distributed	68
5.2 mean range error vs (r, θ) . (a) large error at high angles and range, (b) overall shape	68
5.3 range error σ vs (r, θ) . (a) outliers/large std dev at high angles and range, (b) overall shape	69
5.4 polynomials fitted to range error mean & standard deviation data points to model noise	69
5.5 Comparision of (a) measured and (b) simulated surface noise	71

Aims and Contributions

Aims: start new research, exploratory

Outcomes: -naive observer design

-simulation toolbox for scanning laser rangefinder and rigid bodies. -noise model for Hokuyo UBG 04-LX - more complete model (combines effect of range, angle) in conditions tested than existing literature Contributions: ?

Chapter 1

Introduction

OVERVIEW OF RESEARCH, REPORT:

implementation of an observer to solve novel problem - sparse sensor gives dense measurement. dense measurement part of new direction of research into infinite dimensional symmetry preserving observers. CONTEXT

autonomous robots, unstructured environments. Advances in hardware - need improvements in software to fully utilise capabilities of dense sensors. What is needed is observer design methodology. MOTIVATION

Allow for improved convergence, global. RESEARCH GOALS

Exploratory, look into sparse sensor - dense measurements. Build an observer for an infinite dimensional system - in this case, simplified at first. Will explore if infinite dimensional, symmetry preserving implementation would improve performance WHAT IS IN REPORT

Review of literature

Relevant background

simulation implementation

observer design

experimental data - noise model + measurements collected

1.1 Literature Review

should this be a chapter???

The use of dense sensors allows for a more accurate estimation of the state of an infinite-dimensional system such as a complex, real-world environment. The theory of infinite-dimensional observers is required to fully utilise this information. This section will review the current state of design methodologies and implementations for infinite-dimensional observers. Particular focus will be paid to an emerging avenue of research; symmetry-preserving observer design. Recent theory developments in this area have allowed limitations in the global convergence properties of infinite-dimensional observers to be overcome.

1.1.1 Infinite-Dimensional Observers

In many real world systems the dependent variables are functions of one or more spatial variables. An example would be the dynamics of waves in a body of water. The height of the surface varies continuously along the x and y directions. These spatial variables vary continuously, meaning an infinite number of parameters is required to describe the state of the system. Such systems are termed *infinite-dimensional systems*, or *distributed parameter systems*. Their dynamics are modelled by a partial differential equation (PDE).

When a state estimate is required but direct measurement of the state with sensors is difficult or impossible, a *state observer* is employed. A state observer is a filter that provides an estimate of the state of a system using the difference between its measured and predicted outputs. A more detailed description of an observer is provided in section 2.2. An observer for an infinite-dimensional system is called an *infinite-dimensional observer*.

1.1.1.1 Linear Systems

Observer theory for *linear* infinite-dimensional systems has been widely studied. The techniques used are typically extensions of Luenberger observers and Kalman filter methods used to observe finite dimensional systems.

A simplified approach is to use a spatial discretisation method such as finite difference or finite element to reduce the infinite-dimensional system to a finite-dimensional one. From here, finite-dimensional observer design techniques can be used. This is known as the

early lumping method, and was employed by Stavroulakis [1] who implemented a finite-dimensional observer as part of a control system for an infinite dimensional systems.

The early lumping approach suffers from *spillover*, a phenomenon where performance is affected by the neglected dynamics of the system[2]. Harkort [3] recently developed an observer based control scheme that reduced this effect by using modelled outputs rather than true measurements to reduce the effect of the neglected dynamics.

More accurate observers can be designed with the *late lumping* approach which uses the infinite-dimensional model of the system in the observer design. The result is an infinite-dimensional observer that is discretised later for practical implementation. These methods are typically extensions of Kalman or Luenberger methods to infinite dimensions.

Early work by Gressang [4] extended the Luenberger observer to infinite-dimensional systems whose state space was an abstract Banach space whose dynamics were defined by an infinitesimal generator of a semigroup. More recently, Smyshlyaev [5] developed an exponentially converging backstepping observer for systems governed by parabolic PDEs. Ramdani introduced forward and backward observers [6] whose convergence properties were investigated by Haine [7].

1.1.1.2 Nonlinear Systems

There is currently no universal approach for observer design for nonlinear infinite-dimensional systems. The most common approach has been to linearise the system, then apply a linear infinite-dimensional observer design. Common linearisation methods are Lyapunov methods, extended linearisation and the Lie-algebraic approach [8].

There has been some progress in infinite-dimensional observer design for special cases of nonlinear systems. For bilinear systems, Xu [9] designed an infinite-dimensional observer that converged for certain inputs. Bounit [10] designed Kalman and Luenberger type observers for infinite-dimensional bilinear systems.

Despite these small advances in special case nonlinear design, the most common design methods for nonlinear infinite-dimensional systems rely on linearisation techniques. These techniques rely on the fact that differentiable functions can be approximated by a first-order Taylor expansion around a point. Luenberger and Kalman methods can be applied to linear approximations of system infinite-dimensional systems around an equilibrium point.

This simplification relies on the dynamics of system at the point of linearisation being representative of the entire space. In general, this is not necessarily true, and is the biggest limitation in this design technique. The result is that these linearised observers only converge if the initial state estimate is within a local neighbourhood of the true state. Global converge is not guaranteed which severely limits robustness.

Global convergence can be achieved by taking account the symmetries inherent to the system during observer design. A powerful tool for dealing with symmetries is the theory of *Lie groups*. Investigation into *symmetry-preserving* observer design for systems on Lie groups is an active area of research. It promises to produce theoretically validated design principles for nonlinear infinite-dimensional observers, though the majority of research so far has been limited to finite-dimensional observers.

1.1.2 Symmetry-Preserving Observers

The motivation behind symmetry-preserving observers is to take advantage of invariances in the dynamics of the system. The goal is to design an observer around an equilibrium point in such a way that it can be extended converge around a wider set of points.

1.1.2.1 Early work

Geometry conscious observer design is not a new idea. Early investigation by Marcus [11] into algebraic and geometric methods for nonlinear filter design showed promise. A seminal work by Salcudean [12] was the design of an eventually exponential, globally converging observer for the attitude of rigid bodies from orientation and torque measurements. This observer design takes advantage of the simplicity of the quaternion rotation representation and dynamics of rigid body motion.

Another important result that is a precursor to the active research of today is a design method developed by Aghannan & Rouchon [13]. Their invariant observer construction was based on Cartan's moving frame method. Though convergence was proven for a specific problem, the observer convergence for a general case was left an open problem. Maithripala [14] demonstrated the effectiveness of Aghannan & Rouchons' method by incorporating it into the design of an intrinsic observer based controller. Performance was shown to be independent of the coordinate system used to represent the configuration space.

1.1.2.2 Active Research

There are currently two groups actively researching symmetry-preserving observer design. Both have begun to apply symmetry-preserving methods to infinite-dimensional observers.

The work of Bonnabel, Auroux, Rouchon, Martin et al. is a progression of the early results from Aghannan & Rouchon. Their general approach is to first design a Luenberger type observer around an equilibrium point. An invariant frame is used to construct an invariant output error. The observer innovation term respects the symmetries of the system and thus the nonlinear observer is well behaved around a continuum of equilibrium points.

In [15], a design procedure was developed, based on Aghannan & Rouchons' work. Asymptotic stability was achieved, though this required a design procedure tailored to specific nonlinearities of the system and did not apply in a general case. It was shown in [16] that the invariant error equation simplified convergence analysis. The observer's global behaviour improved, having a larger region of attraction in comparison to naively linearised observers. Developments were made to the theory and presented in [17]. For a particular class of invariant system it was shown that the observer converged locally around any trajectory, and global convergence behaviour was independent of trajectory.

Most recently [18], these invariant design methods were applied to an infinite dimensional system. An observer estimating the state of fluid in a water tank where height varies with continuous dependent variables position and time was developed. It was shown to converge more quickly and robustly than previous attempts at infinite dimensional observer designed with Extended Kalman Filter (EKF) methods.

The work of Trumper, Mahony, Hamel, Lageman et al. differs in scope. The methods of Bonnabel et al. are generalised and can be applied to a wide range of systems. In contrast, the work of Trumper et al. is limited to two specific classes of systems, but achieves stronger convergence properties. In [19] nonlinear filters on the Special Orthogonal Group **SO**(3) are used in attitude estimation and the resulting nonlinear observers achieved almost globally stable observer error. Another attitude observer [20] achieved almost globally asymptotic and locally exponential convergence. In [21], the design methodology for 2 classes of systems is presented. The approach taken is to lift the kinematic system onto its symmetry group and design an observer for the lifted system. The Lyapunov method

is used to design the observer innovation term. This methodology simplifies nonlinear observer design and produces observers with strong convergence properties. This group has also begun research on symmetry-preserving infinite-dimensional observers.

The motivation behind the development of infinite-dimensional observers is to allow dense sensors to be fully utilised. In this vein, research presented in a PhD thesis by Zarrouati [22] utilised dense measurements from a camera and depth sensor. An observer was developed from rotation invariant equations for light and depth. Though the sensors took measurements of an infinite dimensional state, a finite dimensional approximation of this state is what was estimated by the observer.

Another recent work by Adarve et al.[23] also uses dense sensing in the estimation of an infinite dimensional state. This result will be examined closely as it is similar in direction to this research.

Adarve et al. design an update-propagation filter to iteratively compute dense optical flow Φ from CCD camera measurements Y . This optical flow is an infinite dimensional state. Rather than computing the optical flow independently at each frame, a two-stage process is used to build it incrementally. The propagation stage uses a non-linear PDE to model the transport of the optical flow in the next time step. The update stage corrects this prediction using the current image.

The iterative filter used in this approach is an observer that estimates the state of the continuous spatio-temporal flow field. By using a dense sensor, the measured image stream can be treated as a continuous, infinite dimensional state. This is in contrast to sparse optical flow computation where the image is modelled as a set of discrete pixel values. However, the flow fields Φ discretised and computed in r in independent regions Ω around a discrete set of control points ξ as shown in Figure 1.1.2.2. Here, this approach differs from that of general infinite dimensional invariant observer. The state is treated as a discrete set of locally continuous states which does not allow for symmetry considerations. This is because the PDE relations in the local regions are invariant to 2D rotation and translation, but the interactions between regions themselves are not.

Discretising Φ and Y at the beginning of the algorithm design means this is an early lumping design approach. Employing a late lumping approach by discretising an infinite dimensional observer would allow the for the rotation and translation invariance of the flow field to be taken advantage of to improve convergence properties.

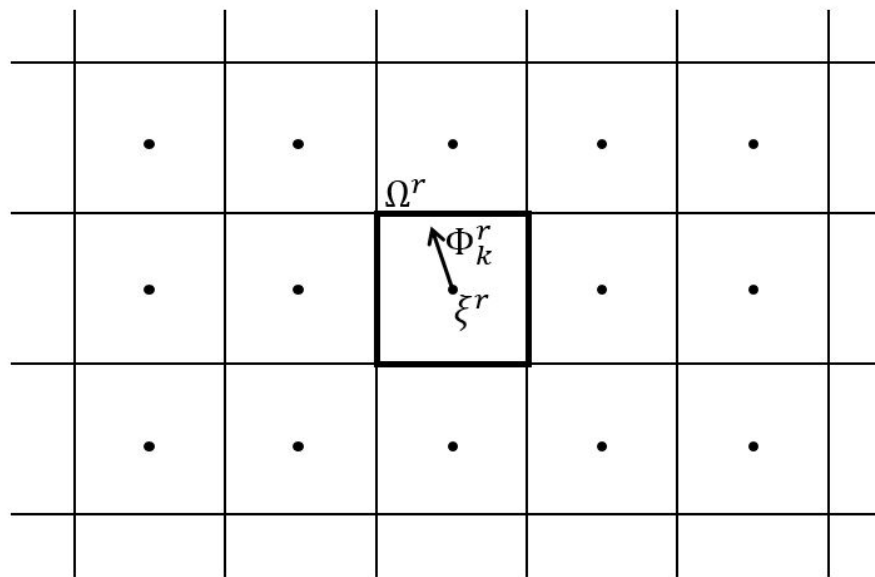


Figure 1.1: Infinite dimensional optical flow discretised and computed in separate, independent regions

The lesson to take from this analysis is that discretisation methods must be carefully chosen in order to preserve the invariance of the system.

Chapter 2

Theoretical Background

2.1 Rigid Body Kinematics

A rigid body is a model of a solid object whose deformation is assumed to be negligible. The distance between every pair of points on the body remains constant. Because such a body does not deform, knowledge of the orientation and position of a reference frame fixed to a rigid body constitutes knowledge of the position of all points. The position of the rigid body is thus defined by the position of a particular point in the body, most commonly its centre of mass. The orientation can be defined using a set of coordinate axes fixed to the body such that its origin coincides with the position point. The theory of Lie groups will be used to describe the kinematics of rigid bodies in this report.

2.1.1 Lie Groups

A Lie group \mathbf{G} is a group whose elements form a differentiable manifold and whose group operation and inverse operation are differentiable. As a group, \mathbf{G} is a set of elements and a group operation. This group operation is a binary operation that combines two elements and is denoted by multiplication: AB or $A \cdot B$ for $A, B \in \mathbf{G}$. Because it is a group, \mathbf{G} satisfies the 4 group axioms:

- **Closure:** The group operation $\mathbf{G} \times \mathbf{G} \mapsto \mathbf{G}$ is a function that maps elements of \mathbf{G} onto itself; $\forall A, B \in \mathbf{G}, AB \in \mathbf{G}$.
- **Associativity:** Elements of \mathbf{G} are associative under the group operation; $\forall A, B, C \in$

\mathbf{G} , $(AB)C = A(BC)$.

- **Identity:** There exists an identity element $I \in \mathbf{G}$ such that $\forall A \in \mathbf{G}$, $IA = AI = A$.
- **Inverse:** For all $A \in \mathbf{G}$ there exists an inverse element $A^{-1} \in \mathbf{G}$ such that $AA^{-1} = A^{-1}A = I$.

Because the Lie group \mathbf{G} is a differentiable manifold, it is locally Euclidean. This means that the neighbourhood around every element of \mathbf{G} can be approximated with a tangent plane. This property allows calculus to be performed on elements of \mathbf{G} .

2.1.1.1 Matrix Lie groups

A matrix Lie group $\mathbf{G} \subset \mathbf{GL}(n)$ is made up of group elements which are $n \times n$ matrices. This work will focus on matrix Lie groups because the form of the exponential map and Lie bracket functions provided below only apply to such Lie groups. Generalised concepts for these functions exist, but a more detailed and relevant description can be given by focusing on matrix Lie groups.

2.1.1.2 Lie algebra

The tangent space at the identity element of a Lie group is called the Lie algebra \mathfrak{g} . It is called the Lie *algebra* because it has a binary operation, known as the Lie bracket $[X, Y]$. For matrix Lie groups the Lie bracket is

$$[A, B] \stackrel{\Delta}{=} AB - BA \quad (2.1)$$

2.1.1.3 The exponential map and logarithm map

The canonical mapping from the Lie algebra \mathfrak{g} to the Lie group \mathbf{G} is called the exponential map:

$$\exp : \mathfrak{g} \rightarrow \mathbf{G} \quad (2.2)$$

Similarly, the logarithm map maps elements from its domain $\mathbf{D} \subset \mathbf{G}$ to \mathfrak{g}

$$\log : \mathbf{D} \rightarrow \mathfrak{g} \quad (2.3)$$

such that for a group element A ,

$$\exp(\log(A)) = A \quad (2.4)$$

For matrix Lie groups, the exponential map and logarithm map correspond to the matrix exponential and matrix logarithm respectively.

2.1.1.4 Infinitesimal generators

The *hat* operator $(\cdot)^\wedge$ can be used to map an n -vector to an $m \times m$ matrix representation, when $\mathbb{R}^{m \times m}$ is isomorphic to \mathbb{R}^n .

$$\begin{aligned} (\cdot)^\wedge : \mathbb{R}^n &\rightarrow \mathbb{R}^{m \times m} \\ x \mapsto x^\wedge &= \sum_{i=1}^n x_i G_i \end{aligned} \quad (2.5)$$

where the set of elements G_i form a basis for $\mathbb{R}^{m \times m}$.

Conversely, the *vee* operator $(\cdot)^\vee$ maps matrices in $\mathbb{R}^{m \times m}$ to vectors in \mathbb{R}^n such that $(x^\wedge)^\vee = x$

$$\begin{aligned} (\cdot)^\vee : \mathbb{R}^{m \times m} &\rightarrow \mathbb{R}^n \\ x^\wedge \mapsto x & \end{aligned} \quad (2.6)$$

For an n -dimensional matrix Lie group, the Lie algebra \mathfrak{g} is a vector space isomorphic to \mathbb{R}^n . The hat operator $(\cdot)^\wedge$ maps vectors $x \in \mathbb{R}^n$ to elements of \mathfrak{g} . For a matrix Lie group \mathbf{G} whose elements are $m \times m$ matrices, the elements of \mathfrak{g} will also be $m \times m$ matrices.

$$\begin{aligned} (\cdot)^\wedge : \mathbb{R}^n &\rightarrow \mathfrak{g} \\ x \mapsto x^\wedge &= \sum_{i=1}^n x_i G_i \end{aligned} \quad (2.7)$$

The basis elements G_i are $m \times m$ matrices known as the infinitesimal generators of \mathbf{G} .

2.1.1.5 Lie bracket and group operation

For Lie groups endowed with the commutative property ($\forall A, B \in \mathbf{G}, AB = BA$), vector addition in the Lie algebra maps to a group operation in the Lie group. For $C = A + B$ where $A, B, C \in \mathfrak{g}$,

$$e^C = e^{A+B} = e^A e^B \quad (2.8)$$

For non-commutative Lie groups, this relationship between the Lie algebra and Lie group operations do not hold. Instead, for $C = \log(e^A e^B)$, C is calculated with the Baker-Campbell-Hausdorff formula:

$$C = A + B + \frac{1}{2}[A, B] + \frac{1}{12}[A - B, [A, B]]\frac{1}{24}[B, [A, [A, B]]] + \dots \quad (2.9)$$

2.1.1.6 Actions

When a group action for a Lie group \mathbf{G} acting on a manifold M is a differentiable map, this is known as a Lie group action. For example, 3D rotations act on 3D points so the Lie group $\mathbf{SO}(3)$ acts on \mathbb{R}^3 . A left action of \mathbf{G} on M is defined as a differentiable map

$$\Phi : \mathbf{G} \times M \mapsto M \quad (2.10)$$

where

- the identity element I acts as the identity on M

$$\Phi(I, m) = m \quad \forall m \in M \quad (2.11)$$

- Group actions compose according to

$$\Phi(m, \Phi(n, o)) = \Phi(mn, o) \quad \forall m, n, o \in M \quad (2.12)$$

2.1.2 $\mathbf{SO}(3)$

A rotation represents the motion of a point about the origin of a Euclidean space. In \mathbb{R}^3 this is a proper isometry: a transformation that preserves distances between any pair of points and has a determinant of +1. The set of all rotations about the origin of \mathbb{R}^3 is

known as the *special orthogonal group* $\mathbf{SO}(3)$. Group elements of $\mathbf{SO}(3)$ can be represented using a special subset of 3×3 invertible matrices and in this case, forms a matrix Lie group. Several rotation representations are described later in this section, but the theory presented below only applies to matrix Lie groups which rely on the rotation matrix representation for group elements.

A rotation matrix \mathbf{R} is a 3×3 matrix that performs a rotation operation when it acts on an element of \mathbb{R}^3 . The properties of \mathbf{R} are described in more detail below.

2.1.2.1 Lie algebra

The Lie algebra $\mathfrak{so}(3)$ is a vector space whose elements represent angular velocities. These elements can be represented with 3×3 skew-symmetric matrices $\boldsymbol{\omega}^\wedge$, where $\boldsymbol{\omega} \in \mathbb{R}^3$ is a 3-vector representing an angular velocity. For $\boldsymbol{\omega} = [\omega_1 \ \omega_2 \ \omega_3]^T$, the skew symmetric representation is given by taking the hat representation of $\boldsymbol{\omega}$

$$\boldsymbol{\omega}^\wedge = \begin{bmatrix} 0 & -\omega_3 & \omega_2 \\ \omega_3 & 0 & -\omega_1 \\ -\omega_2 & \omega_1 & 0 \end{bmatrix} \quad (2.13)$$

Elements of $\mathfrak{so}(3)$ are mapped to $\mathbf{SO}(3)$ according to the exponential map:

$$\begin{aligned} \exp : \mathfrak{so}(3) &\rightarrow \mathbf{SO}(3) \\ \boldsymbol{\omega}^\wedge &\mapsto \exp(\boldsymbol{\omega}^\wedge) \end{aligned} \quad (2.14)$$

where the matrix $\exp(\boldsymbol{\omega}^\wedge) \in \mathbf{SO}(3)$ is a rotation matrix \mathbf{R} .

Conversely, the logarithm map maps 3×3 rotation matrices of $\mathbf{SO}(3)$ to elements of $\mathfrak{so}(3)$:

$$\begin{aligned} \log : \mathbf{SO}(3) &\rightarrow \mathfrak{so}(3) \\ \exp(\boldsymbol{\omega}^\wedge) &\mapsto \boldsymbol{\omega}^\wedge \end{aligned} \quad (2.15)$$

This means that for a rotation matrix \mathbf{R} , $\log(\mathbf{R}) \in \mathfrak{so}(3)$ and represents an angular velocity.

2.1.2.2 Actions

By the group action, elements of $\mathbf{SO}(3)$ rotate points $\mathbf{p} \in \mathbb{R}^3$ about the origin.

$$\begin{aligned}\Phi : \mathbf{SO}(3) \times \mathbb{R}^3 &\rightarrow \mathbb{R}^3 \\ (\mathbf{R}, \mathbf{p}) &\mapsto \mathbf{Rp}\end{aligned}\tag{2.16}$$

2.1.2.3 Rotation representations

There are many conventions by which elements of $\mathbf{SO}(3)$ can be represented. The representations that will be used in this report are described below.

2.1.2.4 Rotation matrices

A 3D rotation matrix \mathbf{R} is an orthogonal 3×3 matrix with a determinant of +1. Since \mathbf{R} is orthogonal, its columns and rows are respectively sets of orthogonal unit vectors and

$$\mathbf{R}^{-1} = \mathbf{R}^T\tag{2.17}$$

The group operation using rotation matrices is simply a matrix multiplication which concatenates the two rotations. The product of two rotation matrices $\mathbf{R}_3 = \mathbf{R}_2\mathbf{R}_1$ is a rotation matrix corresponding to left multiplication by \mathbf{R}_1 followed by \mathbf{R}_2 .

The left action of a rotation matrix \mathbf{R} on a point $\mathbf{p} \in \mathbb{R}^3$ is a left matrix multiplication that rotates \mathbf{p} about the origin.

2.1.2.5 Scaled-axis representation

An orientation in \mathbb{R}^3 can also be represented by a 3-vector $\boldsymbol{\theta}$ whose direction \mathbf{r} represents the axis of rotation and magnitude θ represents the angle of rotation.

$$\boldsymbol{\theta} = \theta\mathbf{r}\tag{2.18}$$

Though scaled-axis vectors are not typically used to perform rotations, Rodrigues' rotation

formula efficiently converts scaled-axis vectors to rotation matrices:

$$\mathbf{R}_\theta = \mathbf{I} + [\mathbf{r}]_\times \sin \theta + ([\mathbf{r}]_\times)^2 (1 - \cos \theta) \quad (2.19)$$

Elements of $\mathfrak{so}(3)$ are typically represented with the hat representation $\boldsymbol{\omega}^\wedge$ of a scaled-axis vector $\boldsymbol{\omega}$, where the magnitude $|\boldsymbol{\omega}|$ corresponds to the angular velocity about the axis $\boldsymbol{\omega}/|\boldsymbol{\omega}|$.

2.1.2.6 Rotation quaternions

Quaternions are an extension of complex numbers. The set of unit quaternions can be used to represent $\mathbf{SO}(3)$, and will be referred to as the set of rotation quaternions. A rotation quaternion \mathbf{q} is a 4-tuple of real numbers that encode the same information as the scaled-axis representation. \mathbf{q} is often described in terms of its first element w - the scalar part, and the remaining elements x, y and z - the vector part. Given an axis of rotation \mathbf{r} and an angle of rotation θ :

$$\mathbf{q} = \begin{bmatrix} w \\ x \\ y \\ z \end{bmatrix} = \begin{bmatrix} w \\ \mathbf{v} \end{bmatrix} = \begin{bmatrix} \cos(\theta/2) \\ \sin(\theta/2)\mathbf{r} \end{bmatrix} \quad (2.20)$$

In general, the quaternion inverse is given by

$$\mathbf{q}^{-1} = \frac{1}{w^2 + x^2 + y^2 + z^2} \begin{bmatrix} w \\ -x \\ -y \\ -z \end{bmatrix} \quad (2.21)$$

For unit magnitude rotation quaternions the inverse represents a rotation by $-\theta$ and is given by

$$\mathbf{q}^{-1} = \begin{bmatrix} \cos(\theta/2) \\ -\sin(\theta/2)\mathbf{r} \end{bmatrix} = \begin{bmatrix} w \\ -x \\ -y \\ -z \end{bmatrix} \quad (2.22)$$

The group operation is performed with quaternion multiplication which is defined:

$$\mathbf{q}_1 \mathbf{q}_2 = \begin{bmatrix} w_1 \\ \mathbf{v}_1 \end{bmatrix} \cdot \begin{bmatrix} w_2 \\ \mathbf{v}_2 \end{bmatrix} = \begin{bmatrix} w_1 w_2 - \mathbf{v}_1 \cdot \mathbf{v}_2 \\ w_1 \mathbf{v}_2 + w_2 \mathbf{v}_1 + \mathbf{v}_1 \times \mathbf{v}_2 \end{bmatrix} \quad (2.23)$$

As with rotation matrices, quaternion multiplication is associative but not commutative.

The group action rotates a point $\mathbf{p}_0 \in \mathbb{R}^3$ to $\mathbf{p}_1 \in \mathbb{R}^3$ by embedding it as the vector component of a quaternion and applying a conjugation operation with \mathbf{q} . The rotated vector \mathbf{p}_1 can be extracted as the vector component of the resulting quaternion.

$$\begin{bmatrix} 0 \\ \mathbf{p}_1 \end{bmatrix} = \mathbf{q} \begin{bmatrix} 0 \\ \mathbf{p}_0 \end{bmatrix} \mathbf{q}^{-1} \quad (2.24)$$

2.1.3 SE(3)

The special Euclidean group **SE**(3) represents rigid transformation in \mathbb{R}^3 . This is a matrix Lie group whose elements comprise the set of all rigid transformations in \mathbb{R}^3 and can be represented with 4×4 matrices of the form

$$\mathbf{S} = \begin{bmatrix} \mathbf{R} & \mathbf{p} \\ \mathbf{0}_{1 \times 3} & 1 \end{bmatrix} \quad (2.25)$$

where $\mathbf{R} \in \mathbf{SO}(3)$ and $\mathbf{p} = [p_x \ p_y \ p_z]^\top \in \mathbb{R}^3$.

SE(3) is a semidirect product of **SO**(3) and \mathbb{R}^3 . As its group elements contain a rotation matrix and translation vector, **SE**(3) has 6 degrees of freedom and is a 6-dimensional manifold.

2.1.3.1 Lie algebra

The Lie algebra **se**(3) is a vector space whose elements are 4×4 matrices of the form

$$\begin{bmatrix} \boldsymbol{\omega}^\wedge & \mathbf{v} \\ \mathbf{0}_{1 \times 3} & 0 \end{bmatrix} \quad (2.26)$$

where $\boldsymbol{\omega} = [\omega_x \ \omega_y \ \omega_z]^\top \in \mathbf{so}(3)$, representing an angular velocity in scaled axis representation, and $\mathbf{v} = [v_x \ v_y \ v_z]^\top \in T\mathbb{R}^3 \equiv \mathbb{R}^3$, representing a linear velocity vector.

Elements of $\mathfrak{se}(3)$ are mapped to $\mathbf{SE}(3)$ according to the exponential map:

$$\begin{aligned} \exp : \mathfrak{se}(3) &\rightarrow \mathbf{SE}(3) \\ \begin{bmatrix} \boldsymbol{\omega}^\wedge & \mathbf{v} \\ \mathbf{0}_{1 \times 3} & 0 \end{bmatrix} &\mapsto \begin{bmatrix} \mathbf{R} & \mathbf{p} \\ \mathbf{0}_{1 \times 3} & 1 \end{bmatrix} \end{aligned} \quad (2.27)$$

i.e. $\forall \mathbf{T} \in \mathfrak{se}(3)$, $\exp(\mathbf{T}) \in \mathbf{SE}(3)$

Conversely, the logarithm map maps elements of $\mathbf{SE}(3)$ to elements of $\mathfrak{se}(3)$:

$$\begin{aligned} \log : \mathbf{SE}(3) &\rightarrow \mathfrak{se}(3) \\ \begin{bmatrix} \mathbf{R} & \mathbf{p} \\ \mathbf{0}_{1 \times 3} & 1 \end{bmatrix} &\mapsto \begin{bmatrix} \boldsymbol{\omega}^\wedge & \mathbf{v} \\ \mathbf{0}_{1 \times 3} & 0 \end{bmatrix} \end{aligned} \quad (2.28)$$

i.e. $\forall \mathbf{S} \in \mathbf{SE}(3)$, $\log(\mathbf{S}) \in \mathfrak{se}(3)$

2.1.3.2 Actions

$\mathbf{SE}(3)$ group elements acts to perform a rigid transformation on points in \mathbb{R}^3 . This corresponds to a rotation about the origin and a translation. To apply a transformation using the 4×4 matrix elements of $\mathbf{SE}(3)$ to a point $\mathbf{p} = (x, y, z)$ in \mathbb{R}^3 , the point must be represented with homogeneous coordinates as \mathbf{p}'

$$\mathbf{p}' = \begin{bmatrix} \mathbf{p} \\ 1 \end{bmatrix} = \begin{bmatrix} x \\ y \\ z \\ 1 \end{bmatrix} \quad (2.29)$$

The left group action of $\mathbf{SE}(3)$ is now simply a left matrix multiplication of \mathbf{p} :

$$\mathbf{p}'_1 = \mathbf{S}\mathbf{p}'_0 = \begin{bmatrix} \mathbf{R} & \mathbf{p} \\ \mathbf{0}_{1 \times 3} & 1 \end{bmatrix} \begin{bmatrix} \mathbf{p}_0 \\ 1 \end{bmatrix} = \begin{bmatrix} \mathbf{R}\mathbf{p}_0 + \mathbf{p} \\ 1 \end{bmatrix} \quad (2.30)$$

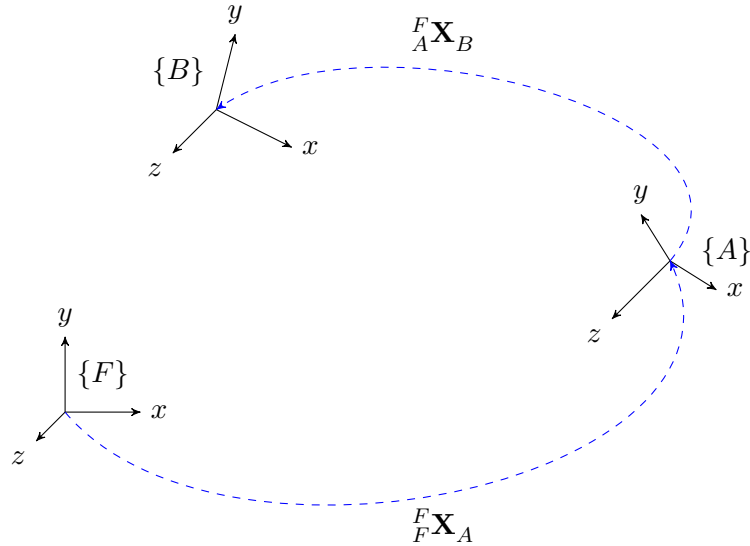


Figure 2.1: Transformations between reference frames $\{F\}$, $\{A\}$ and $\{B\}$ defined with respect to $\{F\}$

2.1.4 Reference Frames

A reference frame is a system of coordinates that is used to uniquely identify points on a manifold. This report will deal with reference frames on \mathbb{R}^3 , that are used both to define the position of a point and the pose of a rigid body in 3D space. Such a reference frame is represented by an element of $\mathbf{SE}(3)$.

The notion of an inertial reference frame is introduced here. This will be defined as a reference frame that is stationary for the purpose of the problem being described. The convention used will be to denote the inertial reference frame as $\{F\}$.

Consider the three reference frames shown in Figure 2.1, denoted $\{F\}$ (the inertial frame), $\{A\}$ and $\{B\}$. The notation $F_A \mathbf{X}_B$ defines the transformation in \mathbf{X} of the reference frame $\{B\}$ with respect to the frame $\{A\}$, defined in the frame $\{F\}$.

For example, $F_A \mathbf{R}_B$ defines the rotation of $\{B\}$ with respect to $\{A\}$, defined in the inertial frame $\{F\}$.

2.1.4.1 Pose

A pose defines an orientation and position in space. The pose of a rigid body is represented by a reference frame fixed to a particular point within the body. The pose of the rigid body

with respect to another reference frame is defined by the relative position and orientation of the two frames. This transformation can be defined with respect to either reference frame and is represented by an element of $\mathbf{SE}(3)$. If a rigid body has orientation aligned with a reference frame $\{B\}$ and position at the origin of $\{B\}$, then the pose of the rigid body with respect to $\{A\}$ and defined in $\{F\}$ is:

$${}^F_A \mathbf{S}_B = \begin{bmatrix} {}^F_A \mathbf{R}_B & {}^F_A \mathbf{p}_B \\ \mathbf{0}_{1 \times 3} & 1 \end{bmatrix} \quad (2.31)$$

2.1.4.2 Point

A point $\mathbf{p} \in \mathbb{R}^3$ in the frame $\{F\}$ is denoted ${}^F \mathbf{p}$ and is expressed as a 3-vector of the weights used to compose it from the basis vectors of $\{F\}$.

$${}^F \mathbf{p} = \begin{bmatrix} {}^F x \\ {}^F y \\ {}^F z \end{bmatrix} \quad (2.32)$$

2.1.4.3 Homogeneous coordinates

To be acted on by an element of $\mathbf{SE}(3)$, a point must be expressed in homogeneous coordinates.

$${}^F \mathbf{p}' = \begin{bmatrix} {}^F \mathbf{p} \\ 1 \end{bmatrix} \quad (2.33)$$

2.1.4.4 Redefining the reference frame of a point

Consider a point in \mathbb{R}^3 defined as the position of the frame $\{A\}$ with respect to the frame $\{F\}$, defined in terms of the frame $\{A\}$. To redefine the point in terms of $\{F\}$, the left action of ${}^F \mathbf{S}_A \in \mathbf{SE}(3)$ is used:

$${}^F \mathbf{p}' = {}^F \mathbf{S}_A {}^A \mathbf{p}' \quad (2.34)$$

2.1.4.5 Concatenating poses

Poses are concatenated by multiplying relative poses.

$${}^F \mathbf{X}_B = {}^F \mathbf{X}_A {}^A \mathbf{X}_B \quad (2.35)$$

2.1.4.6 Redefining the reference frame of a pose

To define a pose transformation matrix in terms of a different reference frame, a matrix conjugation is used.

$${}^A \mathbf{X}_C = ({}^A \mathbf{X}_F) {}^F \mathbf{X}_C ({}^A \mathbf{X}_F)^{-1} \quad (2.36)$$

2.1.4.7 Inverse

Taking the inverse of a pose transformation matrix has the effect of reversing the transformation, but does not alter the frame that the transformation is defined in terms of.

$$({}^A \mathbf{X}_B)^{-1} = {}^B \mathbf{X}_A \quad (2.37)$$

2.1.5 Rigid Body State Representation

The state of a rigid body moving through 3D space can be represented by its linear and angular position, velocity and acceleration. Higher derivatives could be taken but will be ignored for simplicity. The inertial frame is denoted $\{F\}$ and a frame $\{A\}$ is fixed to the pose of the moving body.

The pose of the body with respect to the inertial frame at time t , defined in $\{F\}$ is represented by the **screw** matrix ${}^F \mathbf{S}_A(t) \in \mathbf{SE}(3)$,

$${}^F \mathbf{S}_A(t) = \begin{bmatrix} {}^F \mathbf{R}_A(t) & {}^F \mathbf{p}_A(t) \\ \mathbf{0}_{1 \times 3} & 1 \end{bmatrix} \quad (2.38)$$

where ${}^F \mathbf{R}_A(t) \in \mathbf{SO}(3)$ is a rotation matrix, and ${}^F \mathbf{p}_A(t) \in \mathbb{R}^3$ represents the position of the body defined in $\{F\}$.

The linear and angular velocity of the body at time t with respect to $\{F\}$, defined in the

body-fixed frame $\{A\}$ is represented by the **twist** matrix ${}_F^A \mathbf{T}_A(t) \in \mathfrak{se}(3)$,

$${}_F^A \mathbf{T}_A(t) = \begin{bmatrix} {}_F^A \boldsymbol{\omega}_A^\wedge(t) & {}_F^A \mathbf{v}_A(t) \\ \mathbf{0}_{1 \times 3} & 0 \end{bmatrix} \quad (2.39)$$

where ${}_F^A \boldsymbol{\omega}_A(t) \in \mathfrak{so}(3)$ is an angular velocity in the scaled-axis representation, and the linear velocity is ${}_F^A \mathbf{v}_A(t) \in T\mathbb{R}^3 \equiv \mathbb{R}^3$.

The linear and angular acceleration of the body at time t with respect to $\{F\}$, defined in the body-fixed frame $\{A\}$, is represented by the **wrench** matrix ${}_F^A \mathbf{W}_A(t) \in T\mathfrak{se}(3) \equiv \mathfrak{se}(3)$,

$${}_F^A \mathbf{W}_A(t) = \begin{bmatrix} {}_F^A \boldsymbol{\alpha}_A^\wedge(t) & {}_F^A \mathbf{a}_A(t) \\ \mathbf{0}_{1 \times 3} & 0 \end{bmatrix} \quad (2.40)$$

where ${}_F^A \boldsymbol{\alpha}_A(t) \in T\mathfrak{so}(3)$ is an angular acceleration in the scaled-axis representation, and the linear acceleration is ${}_F^A \mathbf{a}_A(t) \in T^2\mathbb{R}^3 \equiv \mathbb{R}^3$.

From this point on, frames will dropped in the notation. For a body labelled x fixed to a frame $\{A\}$, ${}_F^A \mathbf{S}_A$, ${}_F^A \mathbf{T}_A$ and ${}_F^A \mathbf{W}_A$ will be denoted \mathbf{S}_x , \mathbf{T}_x and \mathbf{W}_x .

2.1.6 Rigid Body Kinematics

The dynamics of the screw, twist and wrench matrices as they are defined in section 2.1.5 are governed by the following ordinary differential equations (ODEs),

$$\frac{d}{dt} \mathbf{S}(t) = \mathbf{S}(t) \mathbf{T}(t) \quad (2.41)$$

$$\frac{d}{dt} \mathbf{T}(t) = \mathbf{W}(t) \quad (2.42)$$

$$\frac{d}{dt} \mathbf{W}(t) = \mathbf{f}(t) \quad (2.43)$$

where the function $\mathbf{f}(t)$ is known.

2.1.7 Scanning Laser Rangefinder Dynamic Model

A scanning laser rangefinder is a sensor that measures the distance to the nearest object in a certain direction. Consider such a sensor fixed to a moving rigid body. The pose of

the sensor s is defined by \mathbf{S}_s , \mathbf{T}_s and \mathbf{W}_s . The scanning direction of the sensor is a unit vector ${}^A\mathbf{d}(t) \in S^2$ defined in the body fixed frame $\{A\}$.

The sensor provides measurement of the range $r(t) \in \mathbb{R}^{0+}$ from ${}^F\mathbf{p}_A(t)$ to the nearest object in the environment in the direction ${}^F\mathbf{d}(t) = {}^F\mathbf{R}_A(t) {}^A\mathbf{d}(t)$.

The function ${}^A\mathbf{d}(t)$ determines the scanning behaviour of the sensor and depends on the specific model used. The scanning model for the Hokuyo UBG-04LX-FO1 used in this research is provided in section 4.1.2.2.

2.2 State Observers

-observer equations for nonlinear system

PLANT - real system. often infinite dimensional.

MODEL - simplified model of real system.

OBSERVER - estimates state of MODEL

plant/state x , output/measurement y , some systems can have input u

nonlinear system: state governed by ODE

$$\dot{x}(t) = f(x(t), u(t)) \quad (2.44)$$

measurement:

$$y(t) = g(x(t), u(t)) \quad (2.45)$$

$$x \in \mathbb{R}^n, y \in \mathbb{R}^m, u \in \mathbb{R}^p$$

f, g nonlinear functions of dimension n, m respectively

state estimate \hat{x} structure for nonlinear observer

$$\dot{\hat{x}} = f(\hat{x}, u(t)) + L(y(t) - \hat{y}(t)) \quad (2.46)$$

$$\hat{y}(t) = g(\hat{x}(t), u(t)) \quad (2.47)$$

$$\dot{\hat{x}} = f(\hat{x}, u(t)) + L(y(t) - g(\hat{x}(t), u(t))) \quad (2.48)$$

L maps \mathbb{R}^m to \mathbb{R}^n

-mention observability? -mention symmetric preserving, infinite dimensional observers briefly

Chapter 3

Problem Statement

context etc here...

estimation problem - cube pose & size:

A situation in which an infinite dimensional observer would be useful is in the estimation of the pose of an object of size moving in an environment of unknown state. For example, consider an autonomous robot deployed in an agricultural survey, which must determine the position and size of a certain crop. Using a geometric model for the general shape of the crop, an aerial vehicle that could routinely detect and characterise the position and size of specimens would be useful in monitoring growth and during harvesting.

The problem to be investigated is shown in Figure 3.1. A 2D scanning range sensor moves through an environment consisting of a target object of known shape, in this case a rigid cube, and an unknown background which may consist of one or more rigid bodies. The

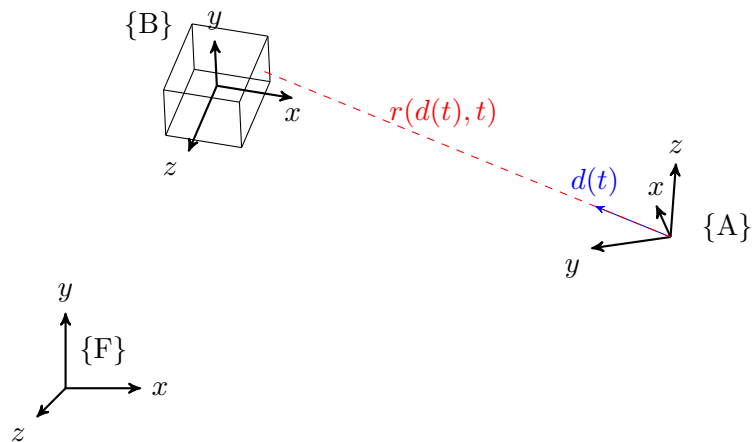


Figure 3.1: caption

state of the sensor is known, but the states of the cube and background environment are unknown. The goal is to use the state of the sensor and the range measurements it provides to estimate the state of the cube.

The frames used to describe the motion of the rigid bodies in this problem are:

- $\{F\}$ - the inertial (fixed) frame. For the purposes of this problem, the inertial frame is a frame whose motion is negligible. For the practical experiment this frame will be fixed to the ground.
- $\{A\}$ - the frame fixed to the sensor. The origin of this frame is the centre of rotation of the sensor's scan direction. The axes of $\{A\}$ are fixed to the sensor according to Figure 4.1 in chapter 4. The transformation from $\{F\}$ to $\{A\}$ at time t is defined by the screw matrix of the sensor $\mathbf{S}_s(t)$.
- $\{B\}$ - the frame fixed to the cube. The origin of $\{B\}$ coincides with the centre of the cube and is aligned so that each axis intersects with the centre of a face of the cube. The transformation from $\{F\}$ to $\{B\}$ at time t is defined by the screw matrix of the cube $\mathbf{S}_c(t)$.

The sensor provides measurements of the range r to the nearest object from the sensor (either the cube or the background) in the direction $\mathbf{d}(t)$. The state of the sensor $\mathbf{X}_s(t)$ is defined as:

$$\mathbf{X}_s(t) = \{{}^F\mathbf{S}_A(t), {}^F\mathbf{T}_A(t), {}^F\mathbf{W}_A(t), {}^A\mathbf{d}(t)\} \quad (3.1)$$

The screw matrix represents the transformation from $\{A\}$ to $\{F\}$, defined in $\{F\}$. The twist and wrench matrices, as well as the scan direction $\mathbf{d}(t)$ are defined in terms of $\{A\}$. For simplicity, this will be denoted

$$\mathbf{X}_s(t) = \{\mathbf{S}_s(t), \mathbf{T}_s(t), \mathbf{W}_s(t), {}^A\mathbf{d}(t)\} \quad (3.2)$$

The direction of measurement ${}^A\mathbf{d}(t)$ varies as a rotation about the z-axis of $\{A\}$. This 2D scanning motion depends on the model of the sensor used and is described in more detail in ADD REFERENCE. For simplification, the motion of the sensor itself with respect to $\{F\}$ will be limited to rotation about the y-axis of $\{F\}$.

The state of cube $\mathbf{X}_c(t)$ is defined as

$$\mathbf{X}_c(t) = \{{}^F_S\mathbf{S}_B(t), {}^F_T\mathbf{T}_B(t), {}^F_W\mathbf{W}_B(t), s\} \quad (3.3)$$

For simplicity, this will be denoted

$$\mathbf{X}_c(t) = \{\mathbf{S}_c(t), \mathbf{T}_c(t), \mathbf{W}_c(t), s\} \quad (3.4)$$

The range measurements do not indicate whether the object detected is the cube or a background object. Though the pose of the cube and environment remain unknown, for simplification, it is assumed that either:

- the cube is within a distance r_{max} from the sensor and background objects are at least a distance r_{max} away
- these target and background objects do not touch or overlap and their surfaces are continuous functions on \mathbb{R}^3

For simulated data, only the first assumption is necessary. For experimental data sets the environment is more complex so the second assumption is required to identify range measurements corresponding to the cube.

The aim is to design an observer which estimates the state of the cube from the pose of the sensor, as well as scan direction \mathbf{s} and range r . Ground truth range unavailable to observer - Will use range measurements \tilde{r} and measurement prediction \hat{r} . Observer function f such that:

$$\hat{\mathbf{X}}_c(k+1) = f(\mathbf{X}_s(t), \hat{\mathbf{X}}_c(k), \tilde{r}(t), \hat{r}(t)) \quad (3.5)$$

*RELATE THIS TO BACKGROUND ON OBSERVERS:

-no input, nonlinear system -state to estimate: state of cube -measurement: range, also relates to state of sensor can also think of this as state to estimate is relative state between sensor, cube *convergence - how to quantify performance? -innovation based on prediction and measured ranges SEPARATELY - this is because only trying to observe cube, ignoring environment. infinite dimensional observer would attempt to estimate infinite dimensional depth field, which is a function on sphere which returns depth - continuous. Instead uses knowledge of environment to filter it out. thus, necessary to have separate measurements, or would only be able to apply innovations when both visible - no solution in this case -

couldn't correct size

deliverables:

Chapter 4

Simulation

4.1 Implementation

A simulation toolbox was implemented in Matlab to model scanning laser range-finder measurements and test observer schemes. The main components of the simulation are:

- rigid body trajectory computation;
- solid object modelling;
- range measurement simulation;
- noise modelling;
- observer implementation.

The notation employed here and throughout the rest of the report uses the following conventions:

- *plain text* variables: single values;
- *bold lowercase* variables: vectors;
- *bold uppercase* variables: matrices
- An array formed by replicating a variable \mathbf{a} in an $n \times m$ block array is denoted $\mathbf{a}_{n \times m}$.
- In many cases, a variable such as the sensor position $\mathbf{p}_s(t)$ represents a set of elements, each corresponding to the value at a certain time t . These will be referred to by the form of the value at a single time. For example, a matrix where each column represents a different position vector is used to represent $\mathbf{p}_s(t)$, but it will be described as a vector as this is the form of a single position.

Algorithm 1: Scanning range-finder and state observer simulation

Data:

n_{steps} - no. steps in simulation
 \mathbf{X}_s - sensor pose and scan direction
 \mathbf{X}_e - cube and background pose, points and triangles
 $\hat{\mathbf{X}}_c$ - estimate of the pose and size of the cube
 c - (true/false) current range measurement is of cube or not
 \mathbf{r} - ground truth range
 $\tilde{\mathbf{r}}$ - measured range
 $\hat{\mathbf{r}}$ - predicted range from state estimate
 α - angle of incidence for each range measurement
 \mathbf{m} - index of triangle measured
 θ - scan angle in sensor frame
 Θ - set of scan angles that return range measurement

```

1 begin
2   settings ← loadsettings
3    $\mathbf{X}_s \leftarrow \text{initialisesensor}(settings)$ 
4    $\mathbf{X}_e \leftarrow \text{initialiseenvironment}(settings)$ 
5   initialiseobserver
6   for  $ii \leftarrow 1$  to  $n_{steps}$  do
7     if  $\theta[ii] \in \Theta$  then
8       |  $[\mathbf{r}[ii], \alpha[ii], \mathbf{m}[ii]] \leftarrow \text{computerange}(\mathbf{X}_s[ii], \mathbf{X}_e[ii])$ 
9     end
10   end
11    $\tilde{\mathbf{r}} = \text{addnoise}(\mathbf{r}, \alpha, \mathbf{m}, settings)$ 
12   for  $ii \leftarrow 1$  to  $n_{steps}$  do
13     |  $\hat{\mathbf{X}}_c[ii + 1] \leftarrow \text{estimatestate}(\hat{\mathbf{X}}_c[ii])$ 
14     | if  $\theta[ii] \in \Theta$  then
15       |   |  $\hat{\mathbf{r}}[ii] \leftarrow \text{computerange}(\mathbf{X}_s[ii], \hat{\mathbf{X}}_c[ii])$ 
16       |   |  $c \leftarrow \text{identifyobject}(c, \tilde{\mathbf{r}})$ 
17       |   | if  $c$  then
18         |   |   |  $\hat{\mathbf{X}}_c[ii + 1] \leftarrow \text{updatestate}(\hat{\mathbf{X}}_c[ii + 1], \mathbf{X}_s[ii], \hat{\mathbf{r}}, \tilde{\mathbf{r}})$ 
19       |   | end
20     | end
21   end
22 end

```

A high level description of the simulation is provided in Algorithm 1. First, a settings file is loaded. The most important settings determined here are the trajectories of the sensor and environment objects, the scanning behaviour of the sensor and the observer update function. Next, the sensor class instance is initialised with `initialisesensor`. This requires computation of the pose and scanning directions of the sensor over time. Similarly, initialisation of the environment through `initialiseenvironment` requires computation of the pose of each rigid body comprising it. The surfaces of the bodies are then represented with a set of points and corresponding triangles. The position of each point with respect to the inertial frame $\{F\}$ is computed at each time step. The settings file provides the initial conditions with which the observer is initialised in `initialiseobserver`. Beginning on line 6, the state of the sensor and environment are used to compute the ground truth range measurements \mathbf{r} at each time step. The incidence angle between the scan direction and object, as well as the index of the triangle hit are also stored as they will be required for sensor noise modelling. This is performed with a parallel `for` loop to speed up computation. Line 7 ensures ranges are only computed when the current scan direction is within the sensor's field of view. In line 11, noise is simulated and added to the ground truth ranges to produce the measured ranges $\tilde{\mathbf{r}}$. The `for` loop beginning on line 12 begins the observer simulation. At each time step, `estimatestate` estimates the state of the cube $\hat{\mathbf{X}}_c$ from the previous state with the kinematics model in 2.1.6. From the sensor state \mathbf{X}_s and the estimated state of the cube $\hat{\mathbf{X}}_c$, `computerange` is used to determine the predicted range measurement $\hat{\mathbf{r}}$. The variable c indicates whether the current range measurement corresponds to the cube or the background. On line 16 the measured ranges and previous value of c are used to determine whether the current measurement corresponds to the cube. If it does, the cube state estimate $\hat{\mathbf{X}}_c$ is updated using the previous state estimate, current sensor state, and the predicted and measured ranges.

4.1.1 Rigid Body Motion

To simulate range measurements the pose of the sensor and the objects comprising the environment must be computed at each time step. The computations required to do so can be reduced by taking into account the kinds of motion that must be simulated. This section details how the pose of the sensor and objects is represented and computed, which is used in the functions `initialisesensor`, `initialiseenvironment` and `estimatestate` referenced in Algorithm 1.

The observer actually computes the *relative* position between the sensor and cube and simply uses knowledge of the sensor pose to determine the pose of the cube in the inertial frame. There is no need to simulate complex sensor motions because the motion of the cube can be adjusted to achieve the same result. The only requirement of the sensor motion is that measurements of a large range of the environment are acquired to ensure that the entire target object can be viewed. The scanning behaviour of the sensor is to rotate back and forth about the z -axis of the body fixed frame $\{A\}$. To provide a rectangular field of view, the motion of the sensor is therefore limited to constant velocity rotation about y -axis of inertial frame $\{F\}$.

The environment is modelled with two rigid bodies: a cube to be observed as the target object, and a stationary rectangular prism enclosing the sensor and cube acting as the background. The various cube motions that will be simulated to test the observer's performance can be classed in terms of the wrench matrix of the cube as either

1. $\mathbf{W}_c = \mathbf{0}$
2. $\mathbf{W}_c \neq \mathbf{0}$

For case 1. the wrench and screw are constant so only the initial value is required. It is more efficient to represent the pose of a rigid body with just position and orientation in this case. The pose can be quickly computed by interpolating between an initial and final pose. For case 2. the screw, twist and wrench must be integrated numerically.

4.1.1.1 Interpolation

For the case of zero wrench, the pose of the body can be represented with a position vector \mathbf{p}_i and an orientation quaternion \mathbf{q}_i . A trajectory of k poses at times $\mathbf{t} = [t_1 \ t_2 \ t_3 \ \dots \ t_k]$, is computed by interpolating from an initial pose $\{\mathbf{p}_0, \mathbf{q}_0\}$ to a final pose $\{\mathbf{p}_k, \mathbf{q}_k\}$.

The array of position vectors $\mathbf{P} = [\mathbf{p}_1 \ \mathbf{p}_2 \ \mathbf{p}_3 \ \dots \ \mathbf{p}_k]$ are computed with:

$$\mathbf{P} = (\mathbf{1}_{3 \times k})\mathbf{p}_1 + (\mathbf{p}_k - \mathbf{p}_1) \frac{\mathbf{t} - t_1(\mathbf{1}_{1 \times k})}{t_k - t_1} \quad (4.1)$$

Spherical linear interpolation is used to compute the array of orientation quaternions

$\mathbf{Q} = [\mathbf{q}_1 \ \mathbf{q}_2 \ \mathbf{q}_3 \ \dots \ \mathbf{q}_k]$ at each time step:

$$\mathbf{Q} = \frac{\mathbf{q}_1 \sin((\mathbf{1}_{[1 \times k]} - \mathbf{t})\theta) + \mathbf{q}_k \sin(\mathbf{t}\theta)}{\sin(\theta)} \quad (4.2)$$

where

$$\theta = \cos^{-1}(\mathbf{q}_1 \cdot \mathbf{q}_k) \quad (4.3)$$

This interpolation method is used to compute the trajectory of the sensor. To acquire multiple views of the entire cube, the sensor must pan back and forth several times. This is achieved by first reversing the trajectory and concatenating with the original to produce the looped trajectories \mathbf{P}_{loop} and \mathbf{Q}_{loop} :

$$\mathbf{P}_{loop} = [\mathbf{p}_1 \ \mathbf{p}_2 \ \mathbf{p}_3 \ \dots \ \mathbf{p}_k \ \mathbf{p}_k \ \mathbf{p}_{k-1} \ \mathbf{p}_{k-2} \ \dots \ \mathbf{p}_1] \quad (4.4)$$

$$\mathbf{Q}_{loop} = [\mathbf{q}_1 \ \mathbf{q}_2 \ \mathbf{q}_3 \ \dots \ \mathbf{q}_k \ \mathbf{q}_k \ \mathbf{q}_{k-1} \ \mathbf{q}_{k-2} \ \dots \ \mathbf{q}_1] \quad (4.5)$$

This looped trajectory is repeated k times to produce multiple back and forth scans:

$$\mathbf{P} = (\mathbf{P}_{loop})_{1 \times k} \quad (4.6)$$

$$\mathbf{Q} = (\mathbf{Q}_{loop})_{1 \times k} \quad (4.7)$$

4.1.1.2 Numerical Integration

The time evolution of the screw, twist and wrench is computed iteratively from initial conditions by numerically integrating the ODEs in section 2.1.6. For a rigid body with an associated reference frame $\{X\}$, moving with constant acceleration:

$$\mathbf{S}_X(t + \delta t) = \mathbf{S}_X(t) \exp(\delta t \mathbf{T}_X(t)) \quad (4.8)$$

$$\mathbf{T}_X(t + \delta t) = \mathbf{T}_X(t) + \delta t \mathbf{W}_X(t) \quad (4.9)$$

$$\mathbf{W}_X(t + \delta t) = \mathbf{W}_X(t) \quad (4.10)$$

Though a higher order integration method, such as Runge-Kutta could be used to compute a trajectory that more accurately represents a constant acceleration, this is not strictly necessary. The observer performance is unlikely to be affected by how constant the acceleration is. Furthermore, it is likely that the experimentally collected data will have even larger variations in acceleration.

To simplify the code, the position vector and orientation quaternion are computed from the screw matrix. This allows the same functions to be used in either the interpolation or numerical integration cases. Multiplying the points that make up the rigid objects can also be done more compactly with quaternions.

4.1.2 Sensor modelling: `initialisesensor`

The motion model below is used to compute the pose of the sensor. The scanning model is used to compute the set of scanning directions. These actions are performed in the `initialisesensor` function in Algorithm 1

4.1.2.1 Motion

The state of the sensor $\mathbf{X}_s(t)$ consists of terms corresponding to its motion and scanning operation. Since the motion of the sensor is restricted to zero acceleration, the state of sensor can be computed with the interpolation method and represented with position, orientation and scanning direction.

$$\mathbf{X}_s(t) = \{\mathbf{p}_s(t), \mathbf{q}_s(t), {}^A\mathbf{d}(t)\} \quad (4.11)$$

Since it has a stationary position, the position of the sensor over time is fixed at the origin of the inertial frame $\{F\}$.

$$\mathbf{p}_1 = \mathbf{p}_2 = \mathbf{p}_3 = \dots = \mathbf{p}_k = \begin{bmatrix} 0 \\ 0 \\ 0 \end{bmatrix} \quad (4.12)$$

The sensor rotates between $-\phi$ and ϕ about the y -axis of inertial frame $\{F\}$. Thus, its orientation is computed by interpolating between \mathbf{q}_1 and \mathbf{q}_k with equation 4.2.

$$\mathbf{q}_1 = \begin{bmatrix} \cos(-\phi/2) \\ \sin(-\phi/2) \end{bmatrix} = \begin{bmatrix} \cos(\phi/2) \\ -\sin(\phi/2) \end{bmatrix} \quad (4.13)$$

$$\mathbf{q}_k = \begin{bmatrix} \cos(\phi/2) \\ \sin(\phi/2) \end{bmatrix} = \begin{bmatrix} \cos(\phi/2) \\ \sin(\phi/2) \end{bmatrix} \quad (4.14)$$

4.1.2.2 Scanning

The scanning behaviour of the sensor depends on the particular model used. The *Hokuyo UBG 04-LX* scanning laser range-finder will be modelled as it was the sensor used to conduct experiments in this project. This sensor produces a 785nm laser beam, projected at a precise direction. It measures the characteristics of the reflected beam to determine the position to the nearest object in the direction of the beam. The direction of the laser beam is varied by reflecting it off a rotating mirror. The rotation means that the beam direction effectively rotates with a constant velocity in a single plane. A portion of the field of view of the laser beam is obscured, so measurements will not be returned in a certain region of each revolution.

The vector ${}^A\mathbf{d}(t)$ will be used to model this scanning behaviour. To accurately model this, the following parameters are used:

- field of view Θ : The vector ${}^A\mathbf{d}(t)$ rotates anti-clockwise about the z axis of the sensor frame $\{A\}$. Measurements are only taken when the scan angle about is between $-\theta$ and θ about the $-z$ -axis of the sensor frame $\{A\}$. In practice, the field of view is implemented as the start angle $-\theta$, direction of rotation and angular range 2θ .
- number of scans n_{scans} : This represents the number of scan angles in a single revolution. Since measurements are limited by the field of view of the sensor, the actual number of measurements per second is $n_{ranges} = \frac{2\theta}{2\pi} n_{scans}$. The angular resolution is $d\theta = \frac{2\pi}{n_{scans}}$.

- revolutions per second Ω : This is measured in Hz and gives the length of each time step $d\tau = \frac{1}{n_{scans}\Omega}$
- n_{loops} : The number of back and forth repeats of the sensor trajectory.

From these parameters the scanning direction ${}^A\mathbf{d}(t)$ is created. At each time t , ${}^A\mathbf{d}(t)$ is either a unit vector indicating the direction of measurement in the sensor frame, or has $\mathbf{0}$ magnitude, corresponding to when ${}^A\mathbf{d}(t)$ is outside the field of view and the sensor is not returning a measurement.

$${}^A\mathbf{d}(t) = \begin{cases} \begin{bmatrix} \cos(-\theta + 2\pi t') \\ -\sin(-\theta + 2\pi t') \\ 0 \end{bmatrix} & \text{if } t' \leq \theta/\pi, t' = k\delta\tau \forall k \in \mathbb{N} \\ \mathbf{0}_{3 \times 1} & \text{if } t' > \theta/\pi, t' \neq k\delta\tau \forall k \in \mathbb{N} \end{cases} \quad (4.15)$$

where

$$t' = \mod(t, 1/d\theta) d\theta \quad (4.16)$$

Figure 4.1 shows the frame $\{A\}$ fixed to the sensor and the scan direction ${}^A\mathbf{d}(t)$. At time $t' = 0$, the first scan direction ${}^A\mathbf{d}_0$ has an angular displacement of $-\theta$ about the z -axis from the forward facing x -direction. After each time step $d\tau$, the scan direction rotates by $d\theta$ about the z -axis. There are n_{ranges} scan directions within the field of view of the sensor. The entire revolution is divided into n_{scans} scan directions.

To simulate range measurements, the scan direction is required in the inertial frame $\{F\}$. This is computed by multiplying with the screw matrix of the sensor.

$$\begin{aligned} {}^F\mathbf{d}'(t) &= \mathbf{S}_s(t) {}^A\mathbf{d}'(t) \\ &= {}^F\mathbf{S}_A(t) {}^A\mathbf{d}'(t) \end{aligned} \quad (4.17)$$

4.1.3 Environment Modelling: initialiseenvironment

4.1.3.1 Motion

The pose of each object represents the pose of its centre of mass. As described in section 4.1.1 the pose is computed with interpolation for the case of zero wrench, and numerical

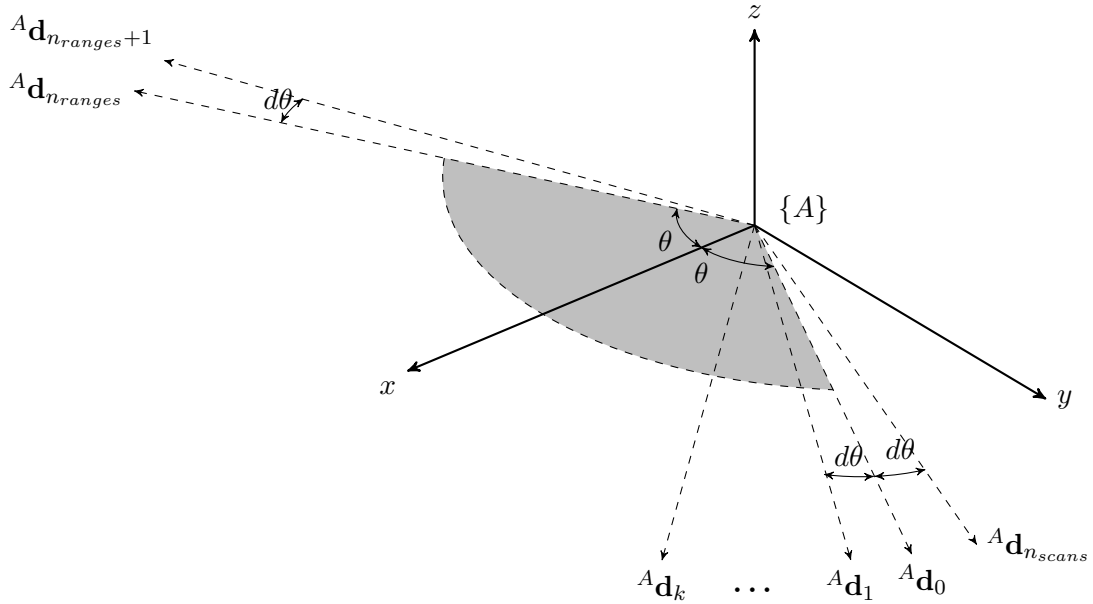


Figure 4.1: Scanning parameters

integration in the case of non-zero wrench. The pose of the objects making up the environment is computed with the function `initialiseenvironment` in Algorithm 1. This function also creates the points and triangles that model the surface of the objects which is described below.

4.1.3.2 Rigid Objects

The environment is represented with two rectangular prisms; the cube and a larger rectangular prism enclosing both the sensor and cube, to represent the background. These objects are modelled as an ordered set of 8 points in the inertial reference frame and an ordered set of 12 triangles formed by these points. Each triangle is represented by a set of 3 integers, indicating the index of the three points that make up its vertices.

The cube points in body frame $\{B\}$ are represented with the matrix ${}^B\mathbf{P}$.

$${}^B\mathbf{P} = \frac{1}{2}s \begin{bmatrix} -1 & -1 & -1 & -1 & 1 & 1 & 1 & 1 \\ -1 & -1 & 1 & 1 & -1 & -1 & 1 & 1 \\ -1 & 1 & -1 & 1 & -1 & 1 & -1 & 1 \end{bmatrix} \quad (4.18)$$

To represent these points in the inertial frame $\{F\}$, ${}^F\mathbf{P}$ is computed by rotating each point with the orientation quaternion of frame $\{B\}$ using equation 2.24 before adding the vector representing the translation of $\{B\}$ from $\{F\}$.

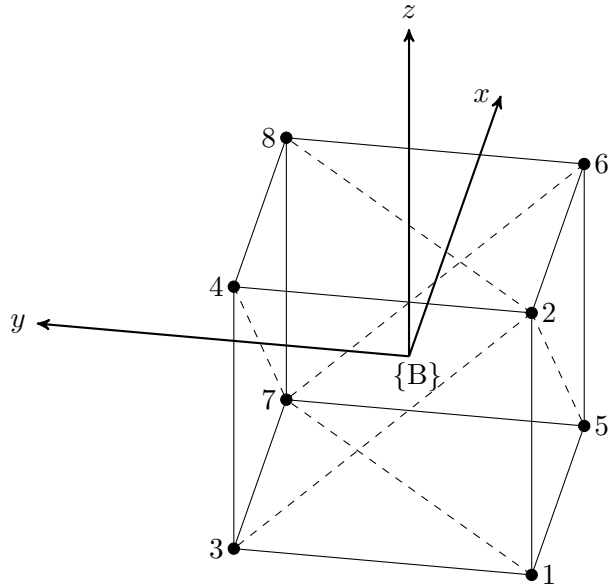


Figure 4.2: Cube modelled with ordered set of points and corresponding triangles

The triangles are represented with the matrix \mathbf{T} . Each triangle is represented by a row. The elements of these rows are the three vertices of the triangle and the index corresponds a point in ${}^F\mathbf{P}$.

$$\mathbf{T} = \begin{bmatrix} 1 & 2 & 3 \\ 2 & 4 & 3 \\ 4 & 3 & 7 \\ 4 & 8 & 7 \\ 5 & 6 & 7 \\ 8 & 6 & 7 \\ 2 & 6 & 5 \\ 2 & 1 & 5 \\ 2 & 6 & 8 \\ 2 & 4 & 8 \\ 1 & 5 & 7 \\ 1 & 3 & 7 \end{bmatrix} \quad (4.19)$$

The points and triangles are shown in Figure 4.2.

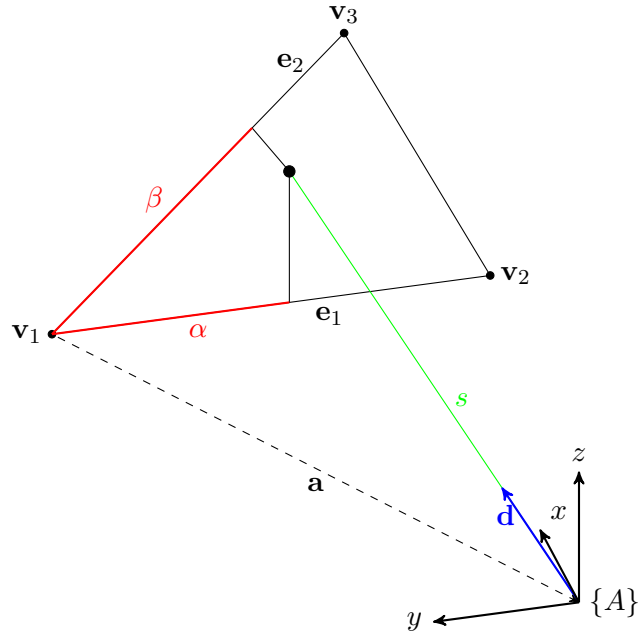


Figure 4.3: Ray-triangle intersection

4.1.4 Measurement Modelling

4.1.4.1 Range Computation: computerange

This section describes the implementation used in the `computerange` function in Algorithm 1.

Given the screw matrix (in the inertial frame) and scan direction (in the body fixed frame) of the sensor, the position and scan direction in the inertial frame are determined. The distance to the nearest environment object from this point, along the scan direction is determined with the Möller-Trumbore ray-triangle intersection algorithm, shown in Algorithm 2.

Figure 4.3 shows a simplified scenario involving the intersection of a ray with a single triangle. In practice, the algorithm is vectorised to compute the intersections with a *set* of triangles. In this vectorised implementation, many variables represent a matrix whose columns are each vectors. These variables will still be described as vectors to emphasise the operation of the Möller-Trumbore algorithm, rather than the specific implementation details.

The output variables are first initialised to the case that there is no intersection with the scanning direction. x is set to `false` and the range, angle and triangle index outputs are

set to return NaN.

On line 8, the set of points \mathbf{P} are indexed using the columns of the triangle matrix \mathbf{T} to extract the three vertices corresponding to each triangle. The vectors representing the edges sharing vertex \mathbf{V}_1 are computed. from triangles and points, extract vertices of each triangle. The vector \mathbf{A} computed on line 14 represents the translation from the ray origin \mathbf{o} to \mathbf{V}_1 .

The collection of vectors \mathbf{B} is computed on line 16 by taking the cross product of the scan direction \mathbf{d} and each edge \mathbf{E}_2 . The determinant δ of the matrix

$$\mathbf{M} = \begin{bmatrix} \mathbf{e}_1 \\ \mathbf{d} \\ \mathbf{e}_2 \end{bmatrix} \quad (4.20)$$

is computed on line 16. This is first used to determine if the scan direction \mathbf{d} lies in the plane of the triangle by checking if the determinant is close to zero. If so, no intersection can occur. The zero determinant values are then set to NaN to avoid a division by zero later.

Beginning on line 21, determinant δ is used to compute the barycentric coordinates α and β , and the distance s from the origin to the triangle plane along the scan direction \mathbf{d} .

The barycentric coordinates are used to determine if the intersection between the scan direction \mathbf{d} and the plane of the triangle lies within the triangle itself.

The vector \mathbf{x} on line 27 now indicates which triangles intersected with the scan direction. \mathbf{x} is used to mask the ranges to the triangles \mathbf{s} , to give \mathbf{r} ; the range to each intersecting triangle.

The minimum range r and triangle index m are determined before computing the angle of incidence θ between \mathbf{d} and the closest triangle.

4.1.4.2 Sensor Noise: addnoise

In Algorithm 1, the function `addnoise` takes the ground truth range measurements and produces the noisy range measurements that the observer will actually receive. The noise

Algorithm 2: Möller-Trumbore ray-triangle intersection

```

input :  $\mathbf{o}$  - ray origin
       $\mathbf{d}$  - ray direction vector
       $\mathbf{P}$  - cube in inertial frame
       $\mathbf{T}$  - triangle matrix
output:  $x$  - True/False - measurement corresponds to object
       $r$  - distance to object in m
       $\theta$  - incidence angle in rad
       $m$  - index of triangle hit

1 begin
2   /* initialise outputs */  

3    $x \leftarrow 0$   

4    $r \leftarrow NaN$   

5    $\theta \leftarrow NaN$   

6    $m \leftarrow NaN$   

7   /* triangle vertexes and edges */  

8    $\mathbf{V}_1 \leftarrow \mathbf{P}[\mathbf{T}[:, 1]]$   

9    $\mathbf{V}_2 \leftarrow \mathbf{P}[\mathbf{T}[:, 2]]$   

10   $\mathbf{V}_3 \leftarrow \mathbf{P}[\mathbf{T}[:, 3]]$   

11   $\mathbf{E}_1 \leftarrow \mathbf{V}_2 - \mathbf{V}_1$   

12   $\mathbf{E}_2 \leftarrow \mathbf{V}_3 - \mathbf{V}_1$   

13   $m = \text{size}(\mathbf{V}_1, 1)$   

14   $\mathbf{A} \leftarrow \mathbf{o}_{[m \times 1]} - \mathbf{V}_1$   

15  /* determinant */  

16   $\mathbf{B} \leftarrow \mathbf{d}_{[m \times 1]} \times \mathbf{E}_2$   

17   $\delta \leftarrow \mathbf{E}_1 \cdot \mathbf{B}$   

18   $y \leftarrow |\delta| \leq 0$   

19   $\delta[y] \leftarrow NaN$   

20  /* barycentric coordinates */  

21   $\alpha \leftarrow (\mathbf{A} \cdot \mathbf{B})/\delta$   

22   $\mathbf{Q} \leftarrow \mathbf{A} \times \mathbf{E}_1$  *(along dim 2)  

23   $\beta \leftarrow (\mathbf{d}_{[n \times 1]} \cdot \mathbf{Q})/\delta$  *(along dim 2)  

24   $s \leftarrow (\mathbf{E}_2 \cdot \mathbf{Q})/\delta$   

25  /* intersection vector */  

26   $\mathbf{z} \leftarrow \mathbf{y}$  and ( $\alpha \geq 0$ ) and ( $\beta \geq 0$ ) and ( $\alpha + \beta \leq 1$ )  

27   $\mathbf{x} \leftarrow \mathbf{z}$  and ( $s \geq 0$ )
28  if any( $\mathbf{x}$ ) then
29     $x \leftarrow 1$ 
30     $\mathbf{x}[\text{not } \mathbf{x}] \leftarrow NaN$ 
31     $\mathbf{r} = \mathbf{s} \circ \mathbf{x}$ 
32     $r = \min(\mathbf{r})$ 
33     $m = \text{find}(\mathbf{r} = r, 1)$ 
34     $\mathbf{e}_1 \leftarrow \mathbf{E}_1[t, :]$ 
35     $\mathbf{e}_2 \leftarrow \mathbf{E}_2[t, :]$ 
36     $\mathbf{n} = \mathbf{e}_1 \times \mathbf{e}_2$ 
37     $\theta = \text{atan2}(|\mathbf{d} \times \mathbf{n}|, \mathbf{d} \cdot \mathbf{n})$ 
38     $\theta = \min(\theta, \pi - \theta)$ 
39  end
40 end

```

function f_s is

$$\hat{r}(t) = f_s(r(t), \theta(t), \phi(k)) \quad (4.21)$$

where $\theta(t)$ is the incidence angle of the measurement, ϕ represents the surface properties of the object k that was measured.

For the Hokuyo UBG-04LX-F01 sensor used, range measurements taken at various distances and incidence angles were used to estimate the noise model f_{UBG} which is provided in section 5.1.

4.1.5 Observer Implementation

FIGURES ARE USED TO EXPLAIN FUNCTIONS. FIGURES THEMSELVES NEED SOME EXPLAINING - IE TRIANGLES ON SURFACE, NOT INSIDE CUBE FOR ORIENTATION

4.1.5.1 Estimate: `estimatestate`

The state of the cube at each time step is estimated using the numerical integration method described in section 4.1.1.2. This state estimation is implemented in the function `estimatestate` in Algorithm 1.

4.1.5.2 Object/background separation: `identifyobject`

The observer update function will use range measurements to estimate the state of the cube \mathbf{X}_c . In order to perform accurately, the observer must only use range measurements that correspond to the cube. The function `identifyobject` in Algorithm 1 uses range measurements and knowledge of the configuration of the environment to separate measurements of the cube and background.

The binary variable c indicates whether the current range measurement corresponds to cube ($c = \text{true}$) or the background ($c = \text{false}$). It is assumed that initially the sensor will be observing the background, so $c_0 = \text{false}$.

The scheme used to identify range measurements corresponding to the cube is shown in Algorithm 3. There are two assumptions that may be used.

1. The *difference assumption* relies on the assumption that the cube and background objects are continuous. Differences in consecutive range measurements larger than Δ_{max} indicate a discontinuity, implying that a new object is being measured. When this occurs, the value of c changes.
2. The *range assumption* is used when the maximum distance to the cube and minimum distance to the background are restricted. Range measurements within r_{max} correspond to the cube while larger ranges correspond to the background.

Algorithm 3: Target/background object separation

```

input : differenceAssumption - true/false
          rangeAssumption - true/false
           $\Delta_{max}$  - max diff between measurements of same object
           $r_{max}$  - max range for cube
           $c$  - true/false - current measurement is of cube
           $\mathbf{r}_{i+1}$  - distance to object at  $t = i + 1$ 
           $\mathbf{r}_i$  - distance to object at  $t = i$ 

output:  $c$  - true/false

1 begin
2   if differenceAssumption then
3     if  $|\mathbf{r}_{i+1} - \mathbf{r}_i| > \Delta_{max}$  then
4        $c = \text{mod}(c + 1, 2)$ 
5     end
6   end
7   if rangeAssumption then
8     if  $\mathbf{r}_{i+1} > r_{max}$  then
9        $c = 0$ 
10    end
11  end
12 end

```

4.1.5.3 Update: updatestate

If the `identifyobject` function identifies a range measurement as corresponding to the cube, the `updatestate` function is used to update the state estimate of the cube $\hat{\mathbf{X}}_c$. $\hat{\mathbf{X}}_c$ is updated using the previous cube state estimate, current sensor state, and sets of measured and predicted range measurements chosen according to a set of indexes $\mathbf{a}(t)$.

$$\hat{\mathbf{X}}_c(k + 1) = f(\mathbf{X}_s(t), \hat{\mathbf{X}}_c(k), \mathbf{r}(\mathbf{a}(t)), \hat{\mathbf{r}}(\mathbf{a}(t))) \quad (4.22)$$

The pose of $\hat{\mathbf{X}}_c$ is corrected by adjusting $\hat{\mathbf{S}}_c$, $\hat{\mathbf{T}}_c$ or $\hat{\mathbf{W}}_c$, or some combination of the three. The orientation is adjusted by rotating about an axis \mathbf{r}_{update} . The position is adjusted by translating in the direction of \mathbf{p}_{update} . \mathbf{r}_{update} and \mathbf{p}_{update} are scaled differently, depending on whether they are applied to $\hat{\mathbf{S}}_c$, $\hat{\mathbf{T}}_c$ or $\hat{\mathbf{W}}_c$. The size update s_{update} is independent of the pose update scheme used.

Input ranges:

A set of four range measurements forming a quadrilateral are used in the state update. The four ranges are chosen with an ordered sequence of indexes $u(t)$. At a time step ii , the set of time steps used is in the update function is

$$\mathbf{u}(ii) = \{ii, (ii - 1), (ii - n_{scans}), (ii - 1 - n_{scans})\} \quad (4.23)$$

It is possible that the measured or predicted ranges do not exist for some time steps in $\mathbf{u}(ii)$, as the range may have corresponded to the background rather than the cube. Thus, the measurement indexes $\tilde{\mathbf{u}}(ii)$ and estimation indexes $\hat{\mathbf{u}}(ii)$ will be subsets of, but not necessarily congruent to $\mathbf{u}(ii)$.

Orientation update:

The method used to correct the orientation of the cube state estimate $\hat{\mathbf{X}}_c$ is shown in Figure 4.4.

In order to estimate the orientation of the cube, at least 3 ranges are required from both the prediction and measurement: $|\hat{\mathbf{u}}| \geq 3$ and $|\tilde{\mathbf{u}}| \geq 3$. If all four indexes are present, the ranges from the last time step $(ii - 1 - n_{scans})$ is ignored.

For both the measurement and prediction, the points of intersection ${}^F\mathbf{P}(\mathbf{u})$ between the set of scanning directions ${}^F\mathbf{D}(\mathbf{u})$ and the cube are computed using the set of range measurements $\mathbf{r}(\mathbf{u})$.

$${}^F\mathbf{P}(\mathbf{u}) = {}^F\mathbf{D}(\mathbf{u})\mathbf{r}(\mathbf{u}) \quad (4.24)$$

The normal to the plane formed by the three points is then computed.

$$\mathbf{n} = [{}^F\mathbf{P}(u_2) - {}^F\mathbf{P}(u_1)] \times [{}^F\mathbf{P}(u_3) - {}^F\mathbf{P}(u_1)] \quad (4.25)$$

Because a cube has 24 regular isometries, it is not necessary to effectively align the reference

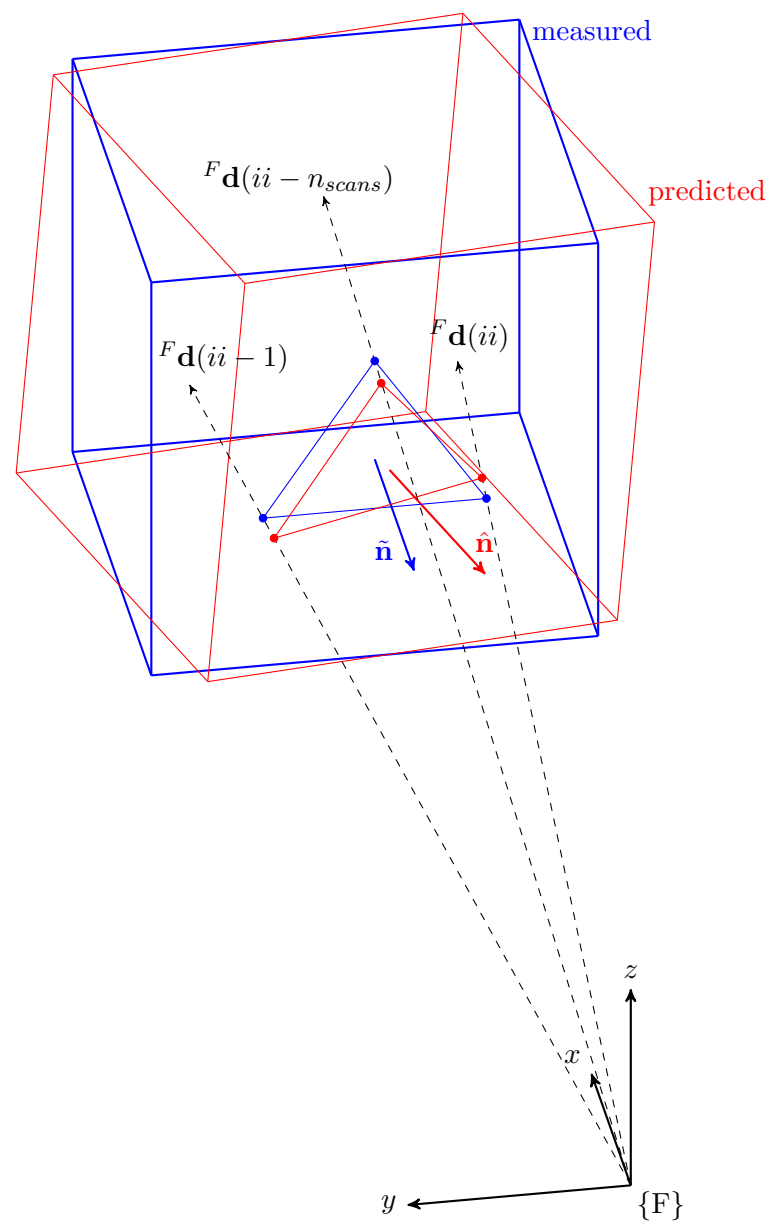


Figure 4.4: Orientation update

frames of the estimated and true cubes. Any face of the estimated cube can be aligned with any face of the true cube, and the maximum rotation correction will be $\pi/4$ radians.

The angle between the two normals ψ is computed as

$$\psi = \text{atan2}(|\hat{\mathbf{n}} \times \tilde{\mathbf{n}}|, \hat{\mathbf{n}} \cdot \tilde{\mathbf{n}}) \quad (4.26)$$

The axis \mathbf{r}_{update} that the estimated cube orientation $\hat{\mathbf{R}}_c$ will be rotated by is computed by taking the cross product of the predicted and measured normals. The direction of rotation is changed if the angle ψ between the two normals is greater than $\pi/4$ radians.

$$\mathbf{r}_{update} = \text{sign}\left(\frac{\pi}{4} - \psi\right) (\hat{\mathbf{n}} \times \tilde{\mathbf{n}}) \quad (4.27)$$

where

$$\text{sign}(x) = \begin{cases} 1 & \text{if } x \geq 0 \\ -1 & \text{if } x < 0 \end{cases} \quad (4.28)$$

To update the screw matrix $\hat{\mathbf{S}}_c$, \mathbf{r}_{update} is converted to a rotation matrix \mathbf{R}_{update} with Rodrigues' rotation formula (equation 2.19). The correction is then applied as:

$$\hat{\mathbf{R}}_c(k+1) = R_{scale} \mathbf{R}_{update} \hat{\mathbf{R}}_c(k) \quad (4.29)$$

To update via the screw or wrench, $\mathbf{r}_{update}^\wedge$ is scaled and then added to the angular velocity or angular acceleration respectively.

$$\hat{\boldsymbol{\omega}}_c^\wedge(k+1) = \hat{\boldsymbol{\omega}}_c^\wedge(k) + \omega_{scale} \mathbf{r}_{update}^\wedge \quad (4.30)$$

$$\hat{\boldsymbol{\alpha}}_c^\wedge(k+1) = \hat{\boldsymbol{\alpha}}_c^\wedge(k) + \alpha_{scale} \mathbf{r}_{update}^\wedge \quad (4.31)$$

The scale factor depends on whether \mathbf{r}_{update} is applied via $\hat{\mathbf{S}}_c$, $\hat{\mathbf{T}}_c$ or $\hat{\mathbf{W}}_c$.

Position update:

The method used to correct the position of $\hat{\mathbf{X}}_c$ is shown in Figure 4.5.

In order to estimate the position of the cube, at least 1 range measurement is required from both the prediction and measurement: $|\hat{\mathbf{u}}| \geq 1$ $|\tilde{\mathbf{u}}| \geq 1$. Additionally, scan directions at time steps ii , $(ii-1)$ and $(ii-1-n_{scans})$ are required. The scan direction ${}^F\mathbf{d}(t)$ must

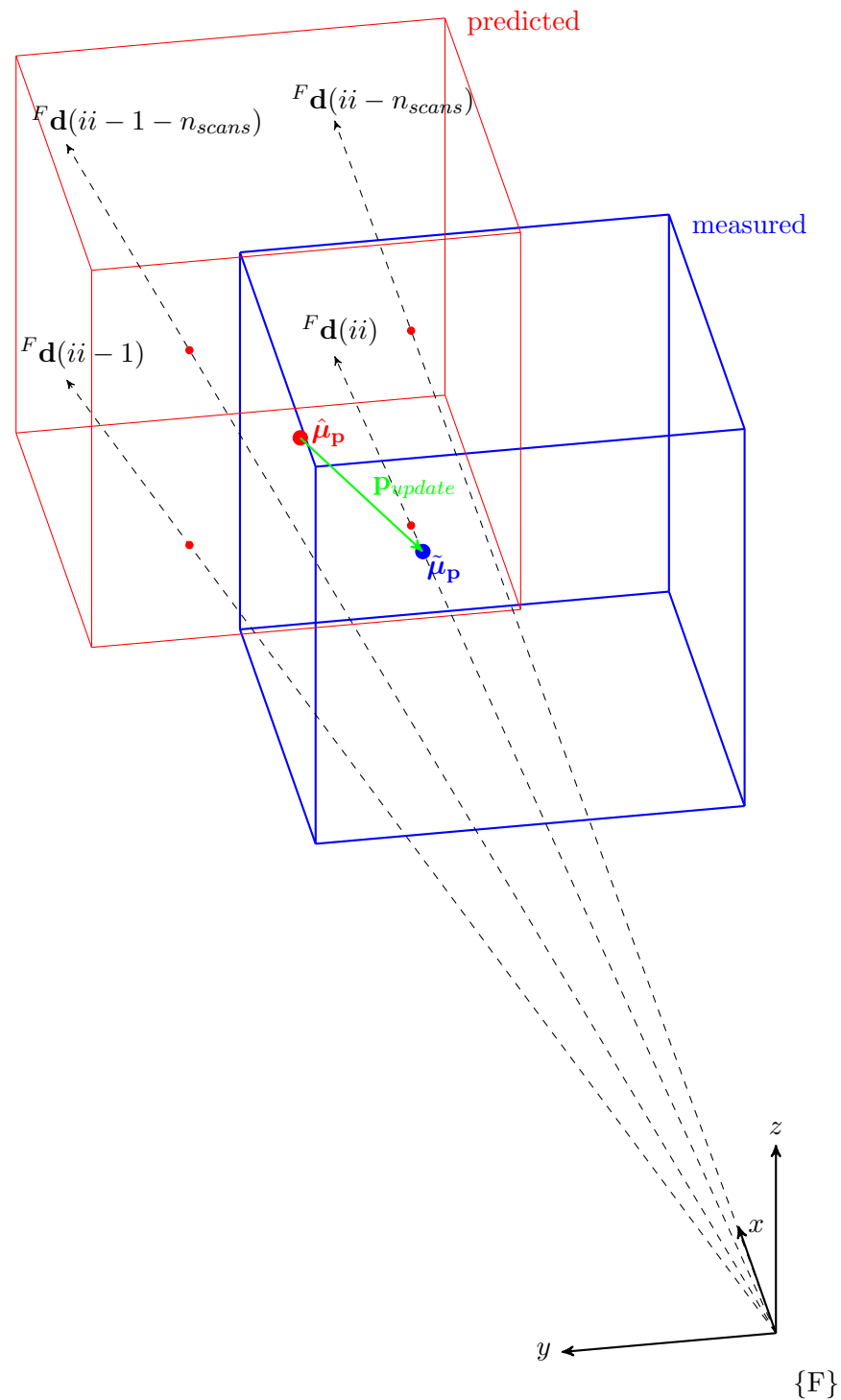


Figure 4.5: Position update

be within the sensor's field of view at these time steps.

The points of intersection are calculated using equation 4.24. The average of these points is computed to give the mean estimated position $\hat{\mu}_p$ and the mean measured position $\tilde{\mu}_p$.

The x, y and z components of the update vector may vary significantly in size due to the scanning behaviour of the sensor. It is necessary to scale the position update vector according to these components. The mean of all predicted and measured ranges μ_r is computed. Four points $\mathbf{p}_0, \mathbf{p}_1, \mathbf{p}_2$ and \mathbf{p}_3 are computed to be used in scaling:

$$\begin{aligned}\mathbf{p}_0 &= \mathbf{p}_s(t) = {}^F_F\mathbf{p}_A(t) \\ \mathbf{p}_1 &= \mu_r {}^F\mathbf{d}(ii) \\ \mathbf{p}_2 &= \mu_r {}^F\mathbf{d}(ii - 1) \\ \mathbf{p}_3 &= \mu_r {}^F\mathbf{d}(ii - 1 - n_{scans})\end{aligned}\tag{4.32}$$

The update vector is computed by scaling the mean intersection points with these four points:

$$\mathbf{p}_{update} = \begin{bmatrix} \frac{1}{|\mathbf{p}_1 - \mathbf{p}_0|} & 0 & 0 \\ 0 & \frac{1}{|\mathbf{p}_2 - \mathbf{p}_1|} & 0 \\ 0 & 0 & \frac{1}{|\mathbf{p}_3 - \mathbf{p}_2|} \end{bmatrix} (\tilde{\mu}_p - \hat{\mu}_p)\tag{4.33}$$

The screw, twist and wrench are corrected using \mathbf{p}_{update} . The scaling factor used depends on whether the update is performed via the screw, twist or wrench.

$$\hat{\mathbf{p}}_c(k + 1) = \hat{\mathbf{p}}_c(k) + p_{scale} \mathbf{p}_{update}\tag{4.34}$$

$$\hat{\mathbf{v}}_c(k + 1) = \hat{\mathbf{v}}_c(k) + v_{scale} \mathbf{p}_{update}\tag{4.35}$$

$$\hat{\mathbf{a}}_c(k + 1) = \hat{\mathbf{a}}_c(k) + a_{scale} \mathbf{p}_{update}\tag{4.36}$$

Size update:

In order to correct the size of the cube, at least 1 range measurement is required from both the prediction and measurement: $|\hat{\mathbf{u}}| \geq 1$ $|\tilde{\mathbf{u}}| \geq 1$. The size update scheme also differs based on the sets predicted and measured ranges.

For the case where a different pattern of ranges is observed ($\hat{\mathbf{u}} \neq \tilde{\mathbf{u}}$), the update method is

shown in Figure 4.6.

The dot product from the vector \mathbf{p}_{update} computed for the position update and the current scan direction is taken:

$$s_{update} = \mathbf{p}_{update} \cdot {}^F\mathbf{d}(ii) \quad (4.37)$$

For the case where the same pattern of ranges is observer ($\hat{a} = \tilde{a}$), the update method is shown in Figure 4.7.

The size update is taken as the difference in the means of the measured and predicted ranges:

$$s_{update} = \tilde{\mu}_r - \hat{\mu}_r \quad (4.38)$$

In both cases, the cube size estimate is updated by scaling s_{update} and adding this to the previous estimate:

$$s(k+1) = s(k) + s_{scale}s_{update} \quad (4.39)$$

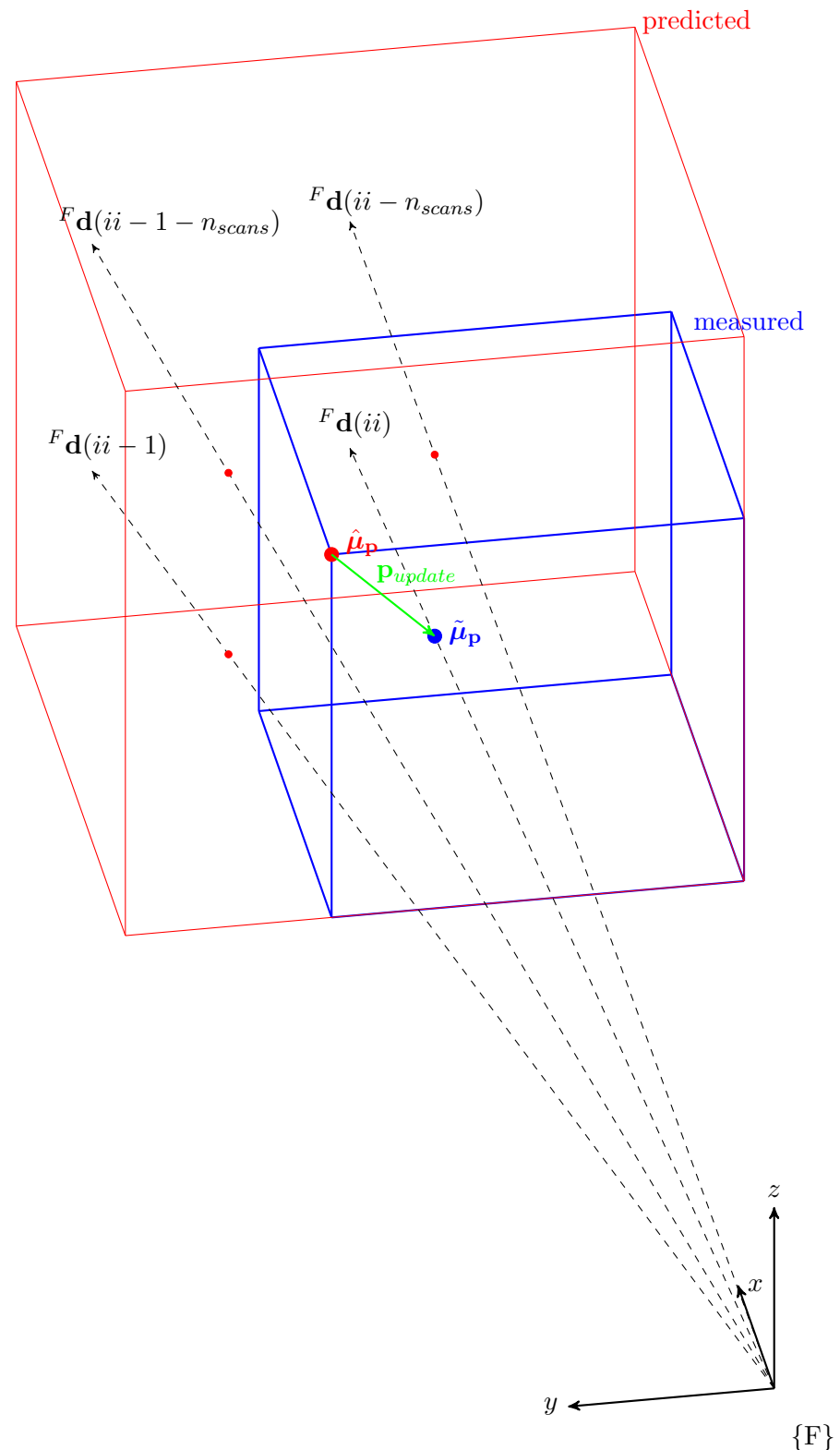


Figure 4.6: Size update - case 1

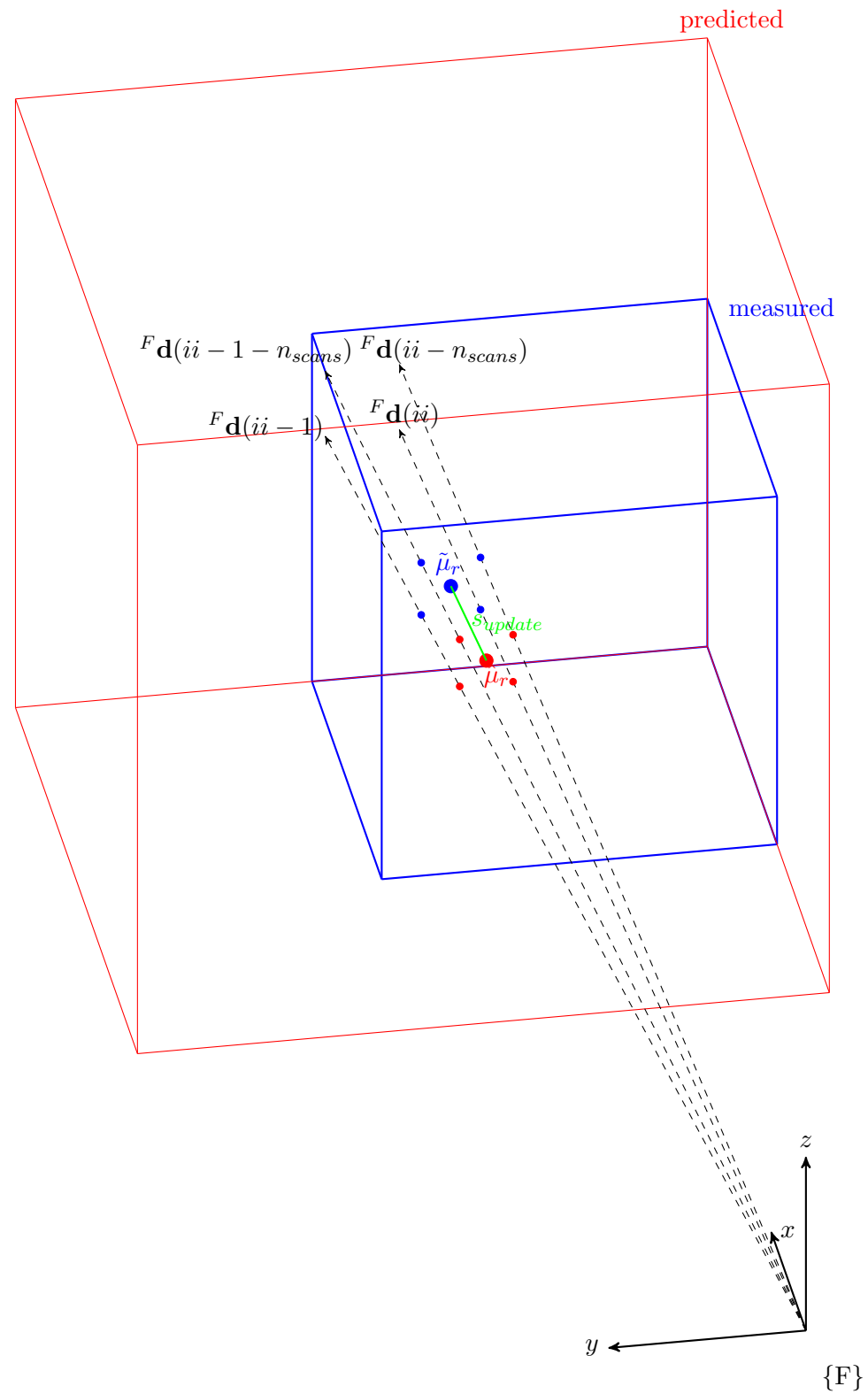


Figure 4.7: Size update - case 2

4.2 Results

4.2.1 testing scheme? think of a title...

tested stationary, rotating, translating, rotating & translating for cases where 1,2,3 faces visible to sensor. tested with and without noise.

Would take too long to perform exhaustive analysis of solution space, testing all the parameters. Instead, will present key results...

4.2.2 Orientation correction

stationary - converges for no noise Figure 4.8.

Doesn't converge to 0 due to noise, but still stable. **THIS DUE TO NOISE FLOOR - INVESTIGATE IF THERE IS TIME - REDUCE NOISE AND SEE IF IT GETS CLOSER** Figure 4.9.

Figure 4.10 - rotating. Updated orientation via screw. Very 'jagged'. Lags slightly, catches up. Figure 4.11 - rotating. Updated orientation via twist. over/undershoots much more than screw. **MENTION: control theory solution - feed forward control. anticipate overshoot, correct before it occurs. FUTURE WORK - DEVELOP OBSERVER THEORY ANALOGUE**

Figure 4.12 - noisy, rotating. Updated orientation via screw, kind of keeps up with rotation but error caused by noise. Figure 4.13 - noisy, rotating. Updated orientation via twist, overshoot error.

4.2.3 Position correction

stationary - works for only 1 face visible. Without noise - Figure 4.14. With noise - 4.15.

doesn't work for 2/3 faces (results 20). Figure 4.16. Requires perpendicular - multiple faces and edges mean update position vector points in wrong direction.

IF THERE IS TIME, ADD TRANSLATION TRACKING

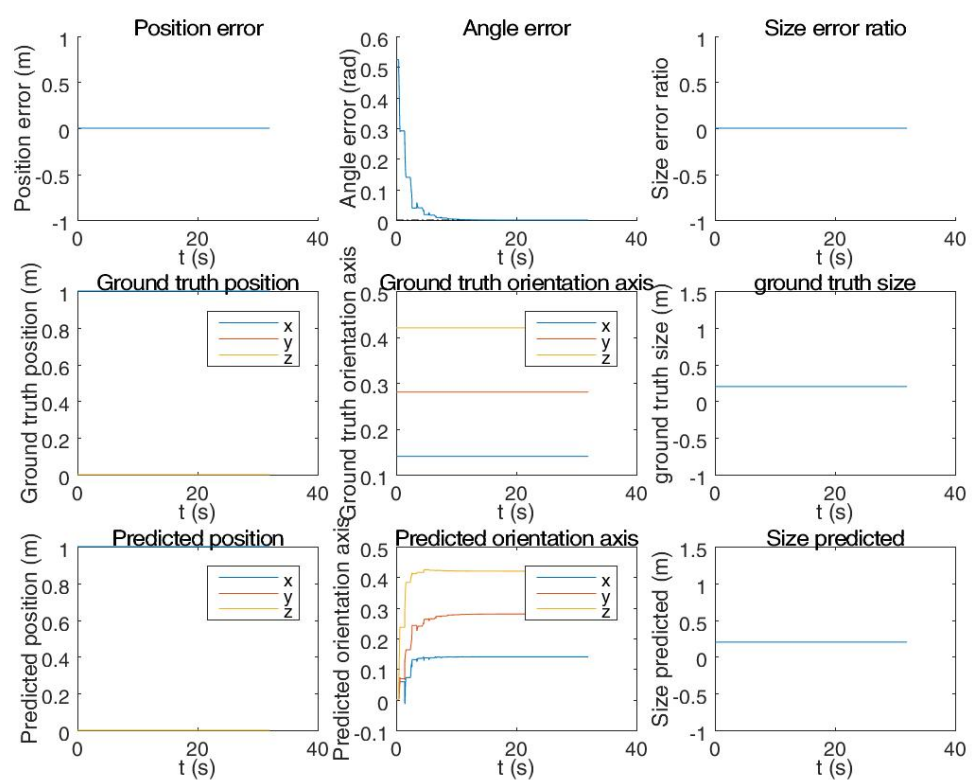


Figure 4.8: Orientation correction - no noise

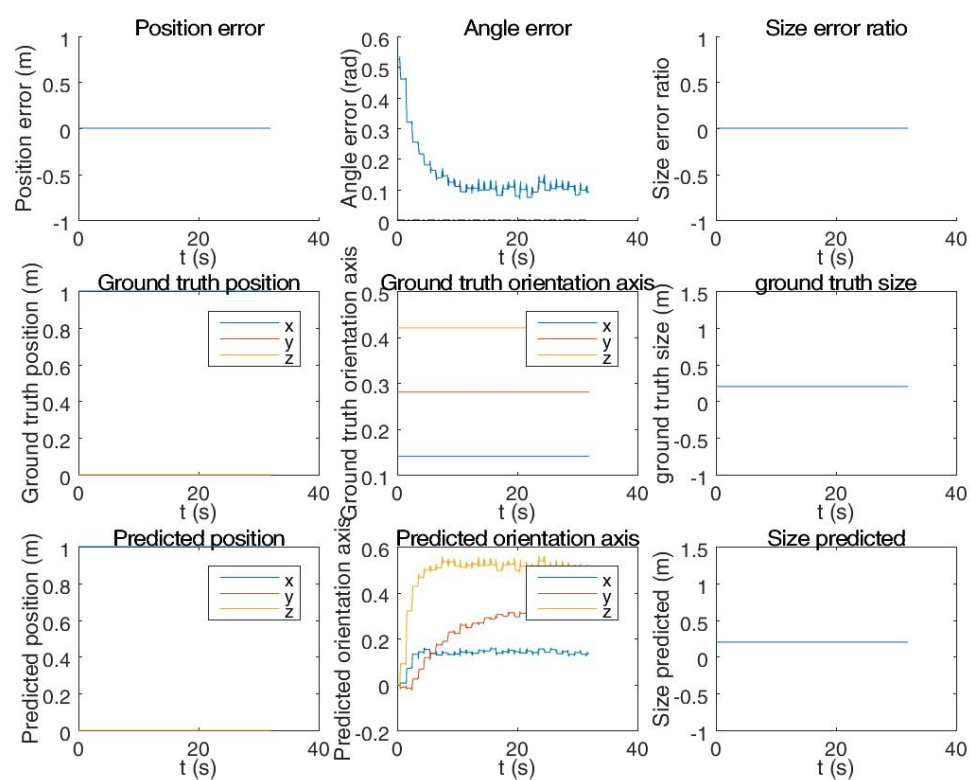


Figure 4.9: Orientation correction - noise

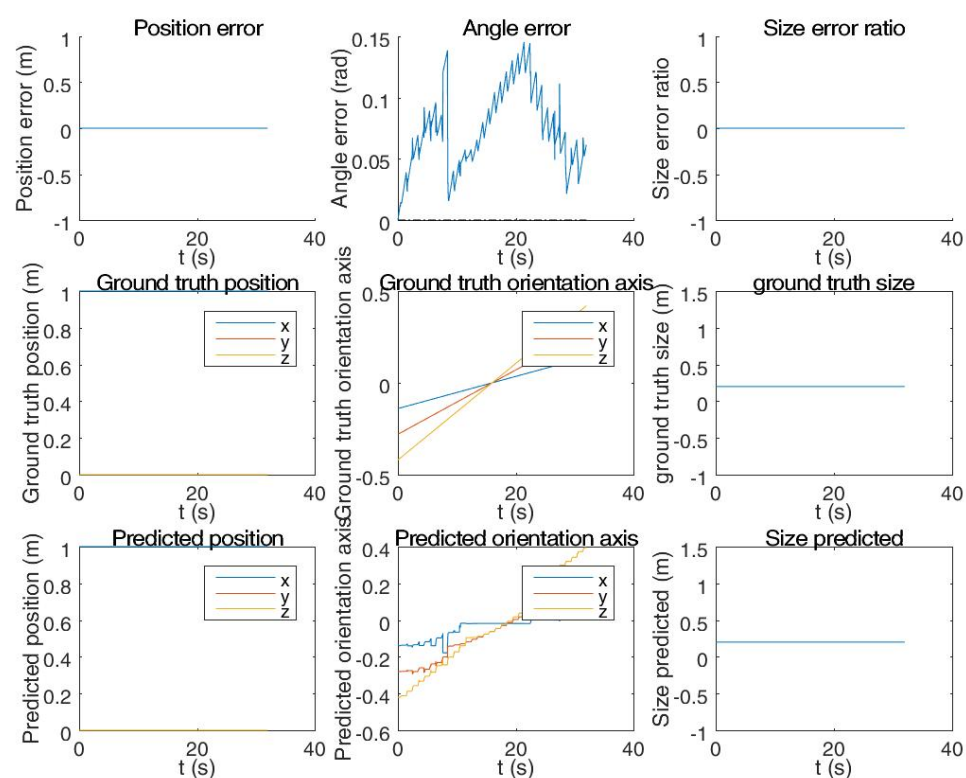


Figure 4.10: rotating - Orientation correction via screw - no noise

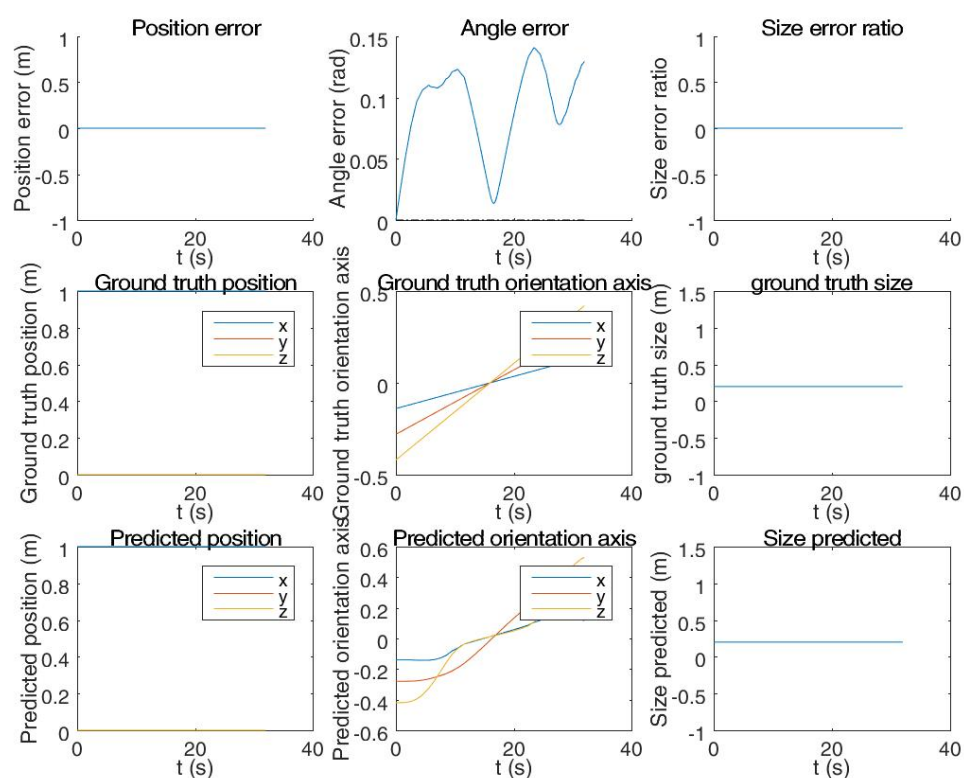


Figure 4.11: rotating - Orientation correction via twist - no noise

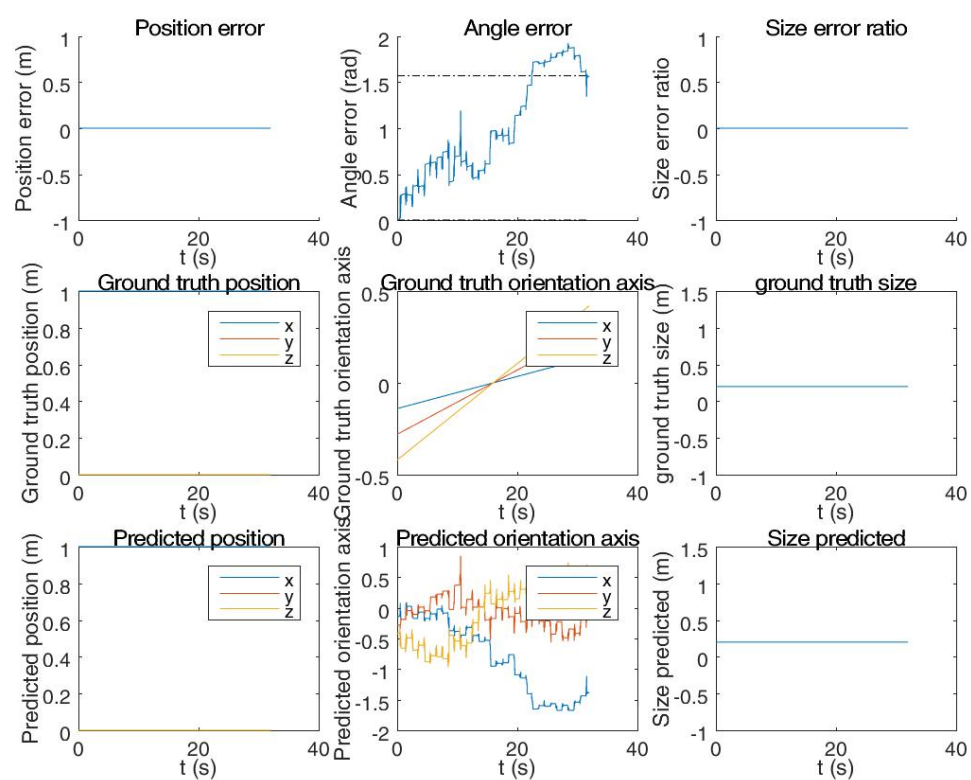


Figure 4.12: rotating - Orientation correction via screw - noise

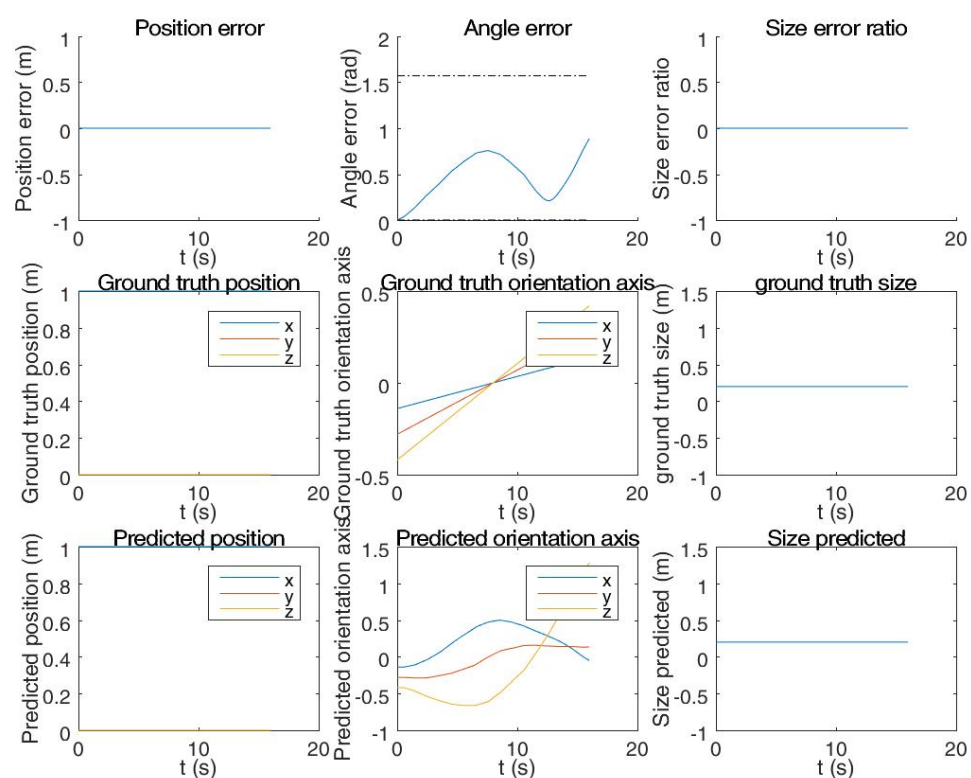


Figure 4.13: rotating - Orientation correction via twist - noise

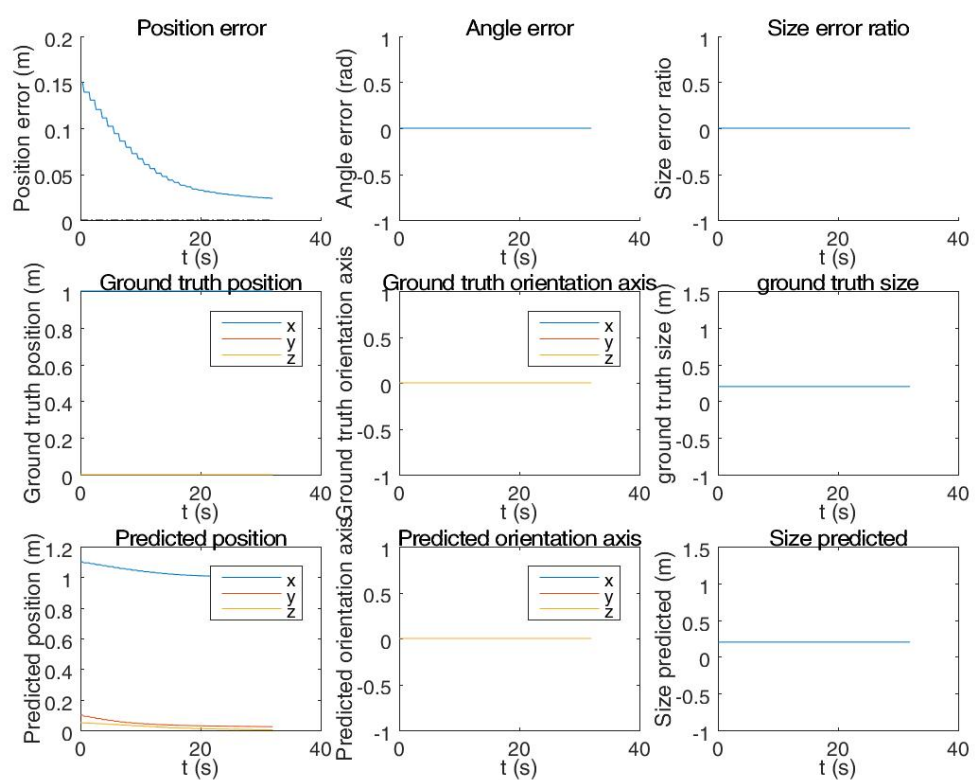


Figure 4.14: stationary, 1 face visible - position correction

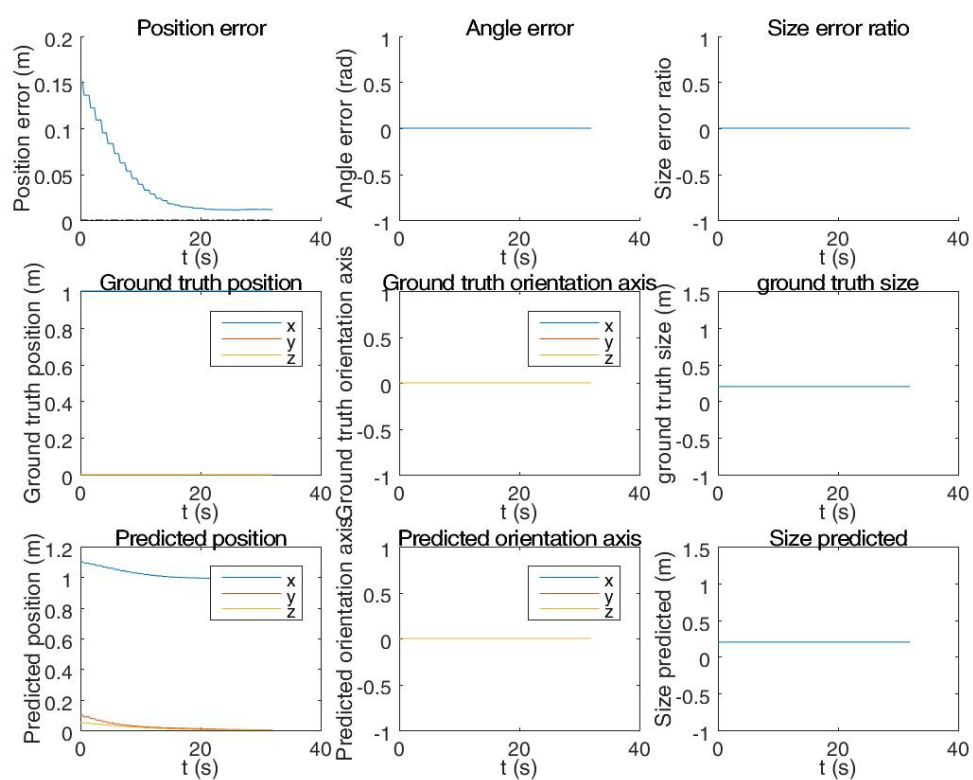


Figure 4.15: stationary with noise, 1 face visible - position correction

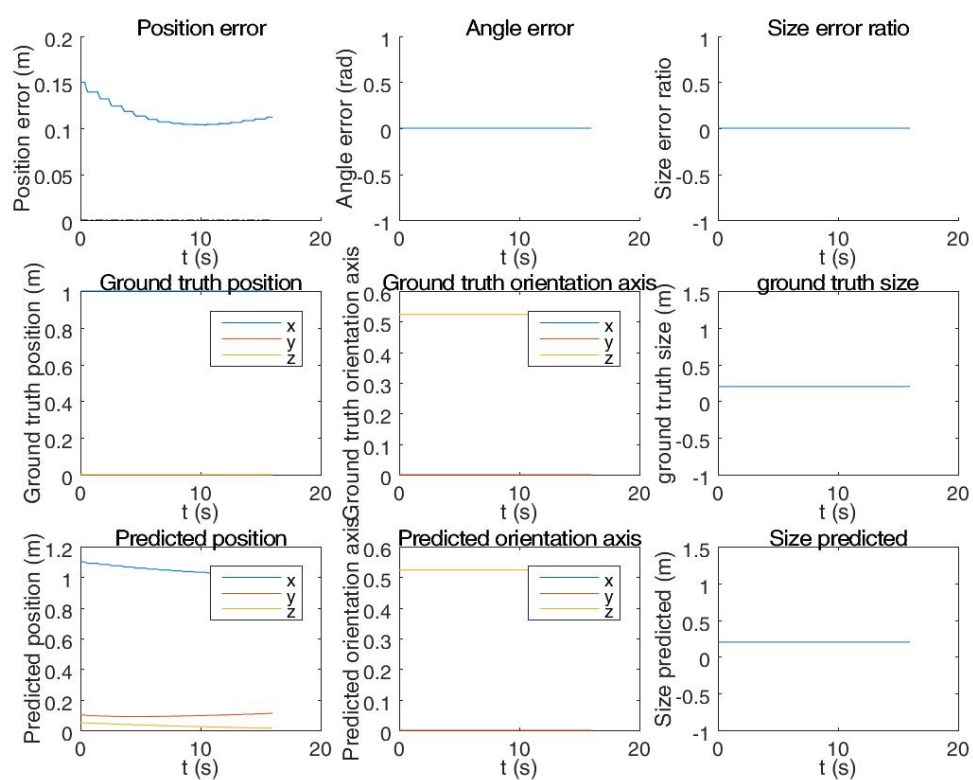


Figure 4.16: stationary with noise, 2 faces visible - position correction doesn't work

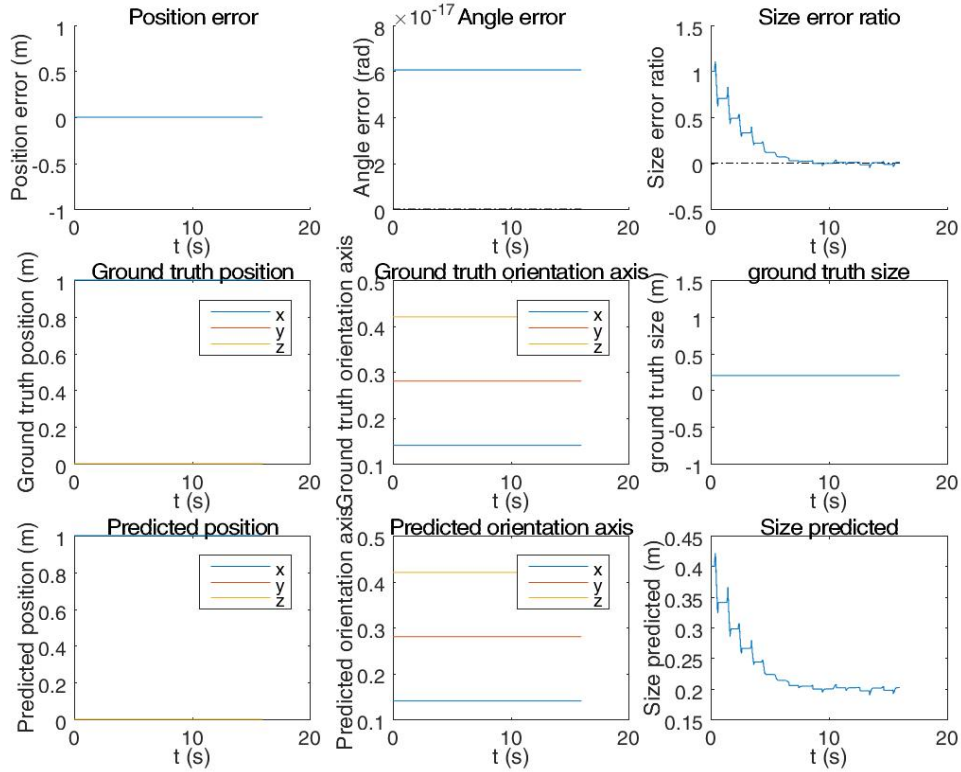


Figure 4.17: stationary with noise, 3 faces visible - size correction

4.2.4 Size correction

works for stationary and moving, noise and no noise, 1,2,3 faces

Figure 4.17 - noise, stationary, 3F visible - size correction

Figure 4.18 - noise, rotating + translating - size correction

4.2.5 Orientation and size

works in same cases orientation alone works

Figure 4.19:stationary, noisy, orientation & size works (results 9).

Figure 4.20 - rotating, no noise, orientation updated via screw, size updated as normal.

Figure 4.21 - rotating, no noise, orientation updated via twist, size updated as normal.

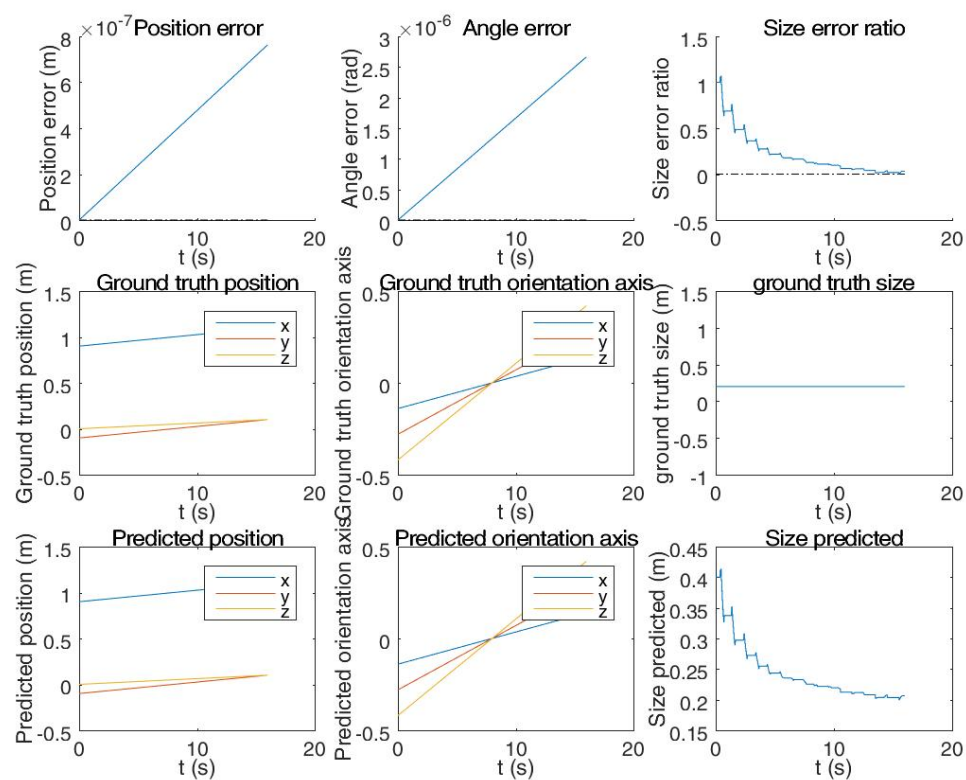


Figure 4.18: rotating + translating with noise, 3 faces visible - size correction

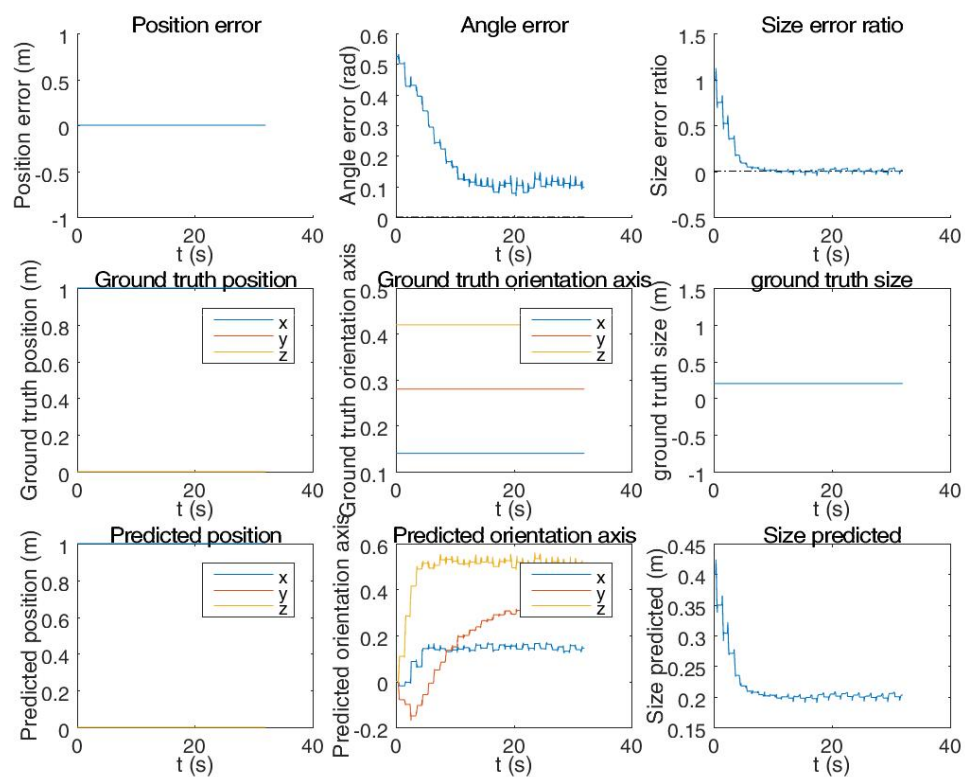


Figure 4.19: stationary with noise, 3 faces visible - orientation and size correction

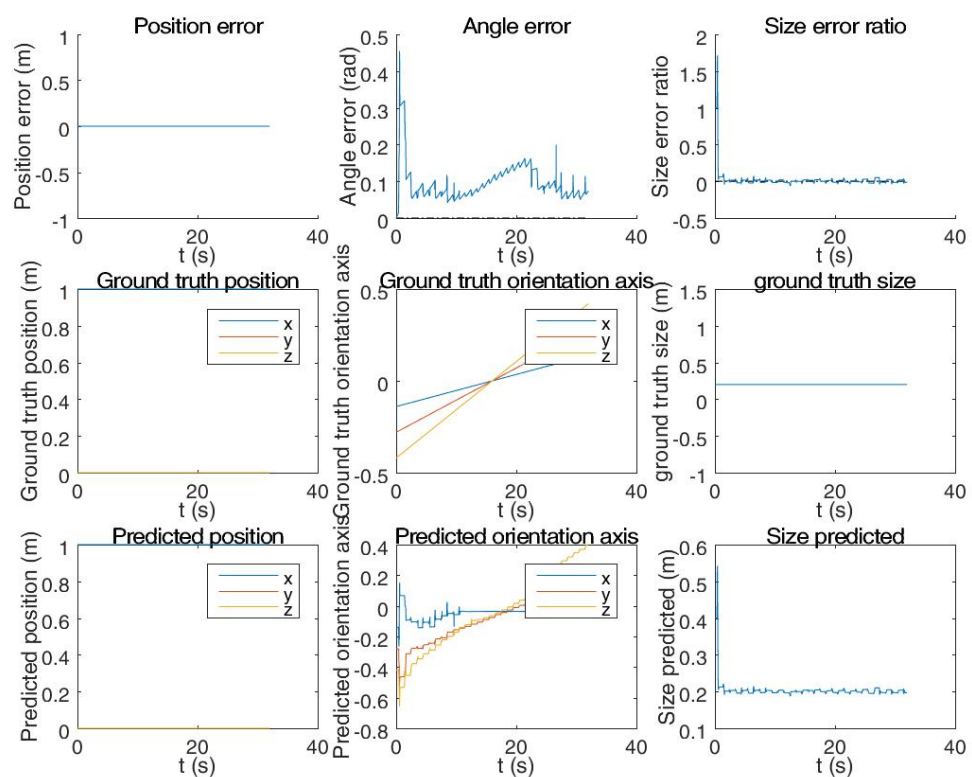


Figure 4.20: rotating with no noise, 3 faces visible - orientation (via screw) and size correction

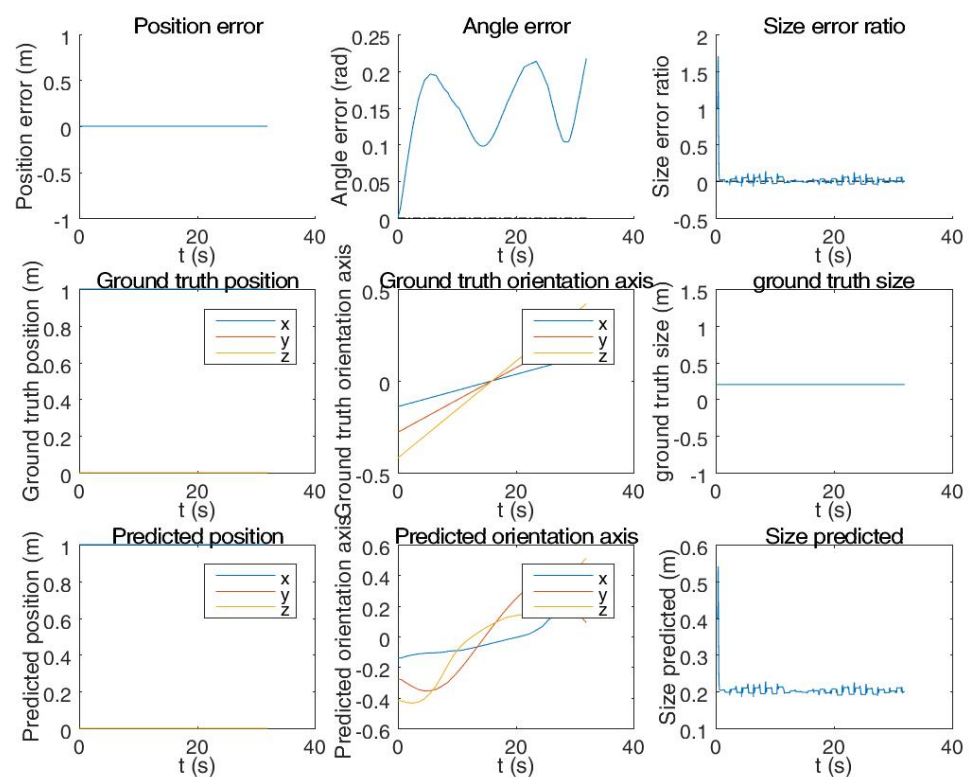


Figure 4.21: rotating with no noise, 3 faces visible - orientation (via twist) and size correction

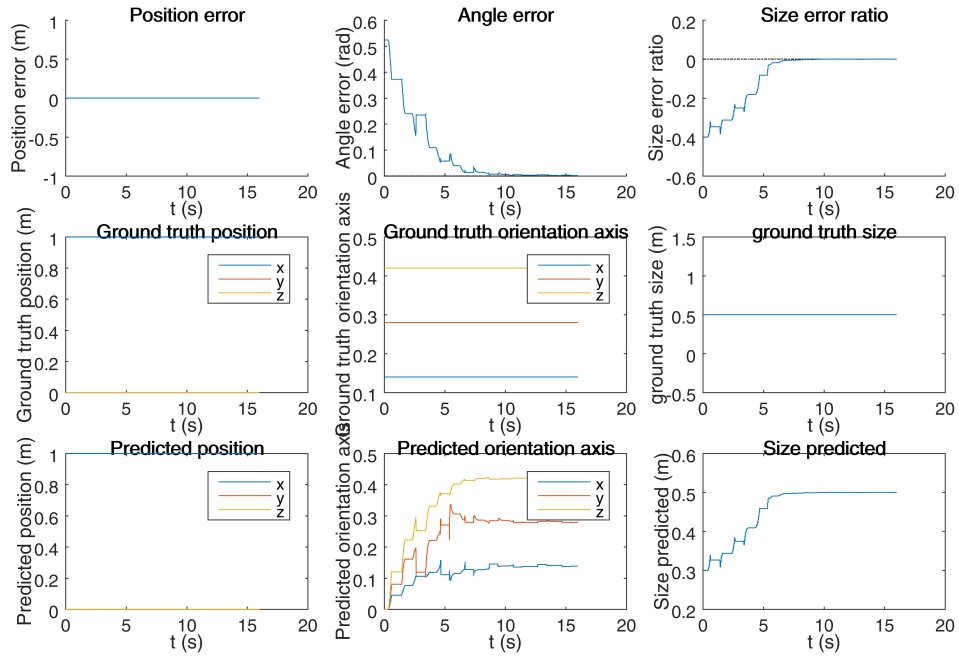


Figure 4.22: Tetrahedron: orientation & size correction

4.2.6 effect of initial conditions

stationary orientation and size, with noise. plot time to within 5% for range of initial angle and size error. see what happens

4.2.7 discussion

Size most robust, then orientation, then position. When combining, performance limited by less robust update.

Observer does not rely on cube shape. Replaced cube with tetrahedron, still works. Figure 4.22.

Seems to be a good approach. To improve, need to fix position. Also, overshoot when adjusting via twist matrix. Twist needs very fine tuning. Instead, do some combination of screw and twist to maximise speed, minimise overshoot.

Chapter 5

Experiment

Sensor:

Hokuyo UBG 04-LX - 2D scanning laser rangefinder. Measures range

Robot arm:

Kinova Jaco - can program to move with and record pose

Target object:

0.1 × 0.1 m MDF cube, spray painted matte white

1. Collected measurements to model sensor noise for simulation
2. Collected measurements of moving cube + measured ground truth cube state - for testing observer with real world conditions

5.1 Sensor Noise Characterisation

motivation - accurate noise model for simulation. In [24], noise characterised but no unified model for range and angle. Furthermore, significant effect from surface colour, texture. Better to develop model for specific case - more accurate practical testing in the future.

5.1.1 Setup

physical setup:

measurement configurations:

-5cm increments from 0.25-1.75m

-vary incidence angle: 0,20,40,60,80 degrees

5.1.2 Results

Similar results to [24]. Difficult to get sensible readings at high angles, Gaussian distributed noise. **Error distribution:** Histograms (Figure 5.1) - range error approximately normally distributed:

Mean range error as function of (range,incidence angle) - Figure 5.2

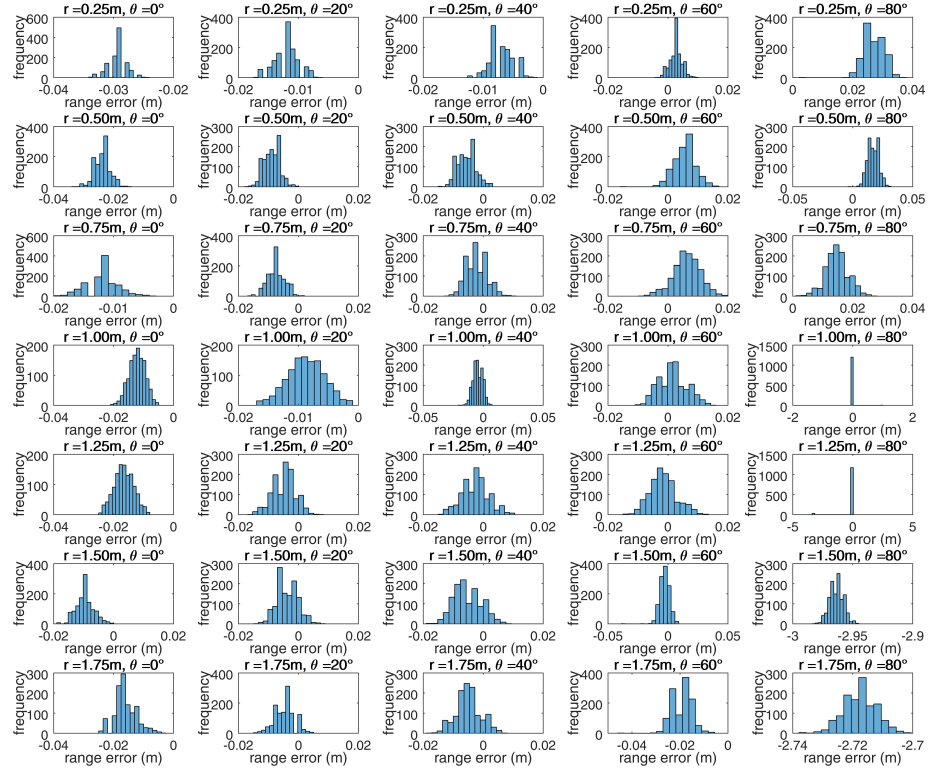
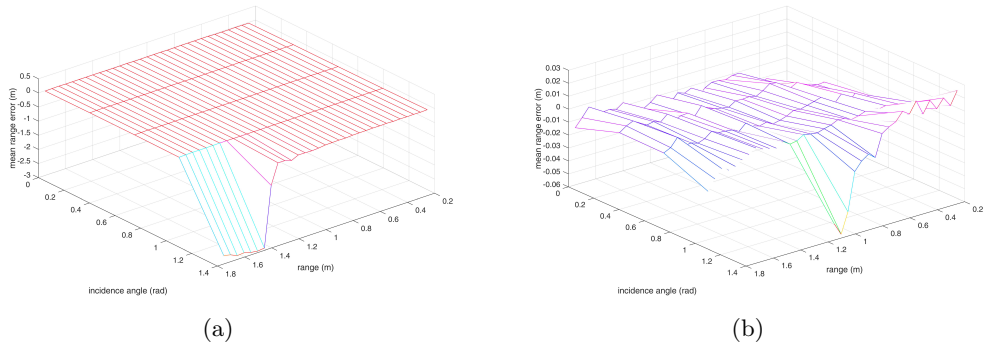
Std dev range error as function of (range,incidence angle) - Figure 5.3

Fitted 4th degree (in x and y) polynomials to data points - Figure 5.4. INCLUDE FIT DATA

Noise Model:

$$\hat{r} = f_s(r, \theta, \phi(k)) = r + \mathcal{N}(\mu, \sigma) \quad (5.1)$$

$$\begin{aligned} \mu = & a_{00} + a_{10}r + a_{01}\theta + a_{20}r^2 + a_{11}r\theta + a_{02}\theta^2 \\ & + a_{30}r^3 + a_{21}r^2\theta + a_{12}r\theta^2 + a_{03}\theta^3 + a_{40}r^4 \\ & + a_{31}r^3\theta + a_{22}r^2\theta^2 + a_{13}r\theta^3 + a_{04}\theta^4 \end{aligned} \quad (5.2)$$

Figure 5.1: $r_{error}(r, \theta)$ approximately normally distributedFigure 5.2: mean range error vs (r, θ) . (a) large error at high angles and range, (b) overall shape

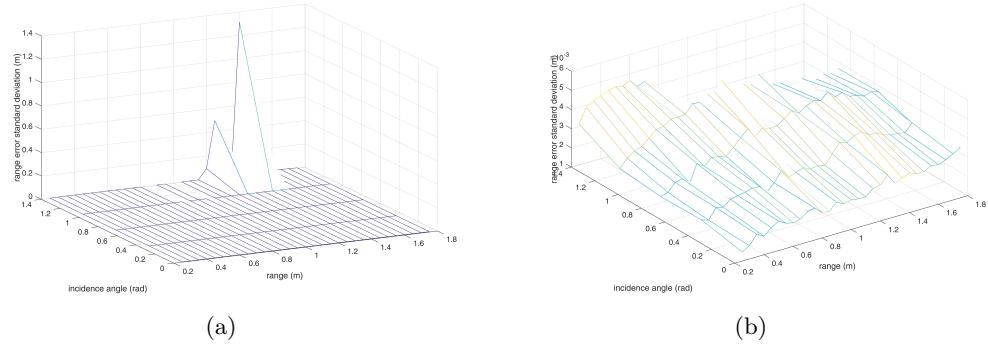


Figure 5.3: range error σ vs (r, θ) . (a) outliers/large std dev at high angles and range, (b) overall shape

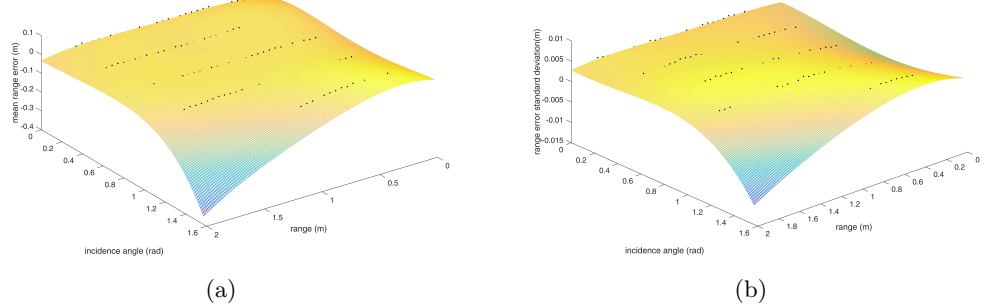


Figure 5.4: polynomials fitted to range error mean & standard deviation data points to model noise

$$\begin{aligned}
\sigma = & b_{00} + b_{10}r + b_{01}\theta + b_{20}r^2 + b_{11}r\theta + b_{02}\theta^2 \\
& + b_{30}r^3 + b_{21}r^2\theta + b_{12}r\theta^2 + b_{03}\theta^3 + a_{40}r^4 \\
& + b_{31}r^3\theta + b_{22}r^2\theta^2 + b_{13}r\theta^3 + b_{04}\theta^4
\end{aligned} \tag{5.3}$$

*outliers ignored in model. if angle > 75 deg and range > 0.8m, range measurement = NaN. EXPLANATION: as angle increases, measured range becomes less than ground truth - due to beam width. part of beam hits part of object that is closer due to angle. However, as angle increases further, not enough light returns to make measurements. At high ranges and angles, measurement is not of object, but due to reflections that take much longer. Measurement ends up being near maximum range or even INF. Instead, will set as NaN - no value returned.

Coefficients in tables 5.1 and 5.2

Table 5.1: a_{ij} coefficients

	j_0	j_1	j_2	j_3	j_4
i_0	-0.06529	0.2126	-0.533	0.4629	-0.1223
i_1	0.2024	-0.1906	0.4006	-0.1791	0
i_2	-0.3074	0.0228	-0.0716	0	0
i_3	0.2053	0.01455	0	0	0
i_4	-0.04912	0	0	0	0

Table 5.2: b_{ij} coefficients

	j_0	j_1	j_2	j_3	j_4
i_0	0.001242	0.2126	-0.01128	0.01162	-0.002746
i_1	0.00352	0.006146	0.01021	-0.007316	0
i_2	-0.005138	-0.00626	-0.0005068	0	0
i_3	0.004067	0.001337	0	0	0
i_4	-0.001092	0	0	0	0

Surface noise: random walk model

have observed error mostly independent of range and angle - seems to be some compensation performed by sensor to get straight lines - range across smooth surfaces that should be appear as straight lines varies regularly. Could be surface properties of objects, though error is larger than expected in this case. Profile of error sinusoidal (regular-ish peaks and valleys), peaks = 5mm deep & 50mm wide approximately

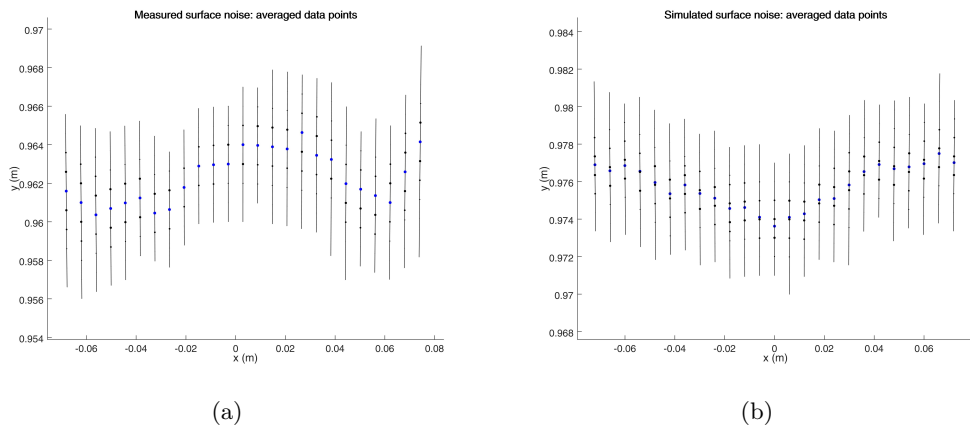


Figure 5.5: Comparision of (a) measured and (b) simulated surface noise

add random walk to each scan

$$error = a \sum_{n=1}^{n_{Steps}} -1 + 2 \lfloor \mathcal{R} \rfloor \quad (5.4)$$

where \mathcal{R} is a random variable following a uniform distribution on $[0,1]$. Chose step size of $a = 0.0005m$ Doesn't work too well over long surfaces (1m) - can get too large sometimes, but fits measured data for small objects like cube

Figure 5.5: comparison of simulated & measured surface noise: **ERROR BARS INSTEAD OF DOTS**. MENTION THAT IT IS FLIPPED, COULD BE OTHER WAY. DUE TO RANDOM WALK.

5.2 Testing Data Collection

5.2.1 Setup

physical setup

configurations/motions:

- stationary

- rotating

- translating

(all above with 1,2,3 faces visible to sensor)

arm forward kinematics → cube pose

estimate sensor angle with horizontal with wall calibration data

5.2.2 Results

observer performance

Chapter 6

Conclusion

refer back to context, literature, motivation

implemented observer - dense sensor.

results promising - dense sensor capable of observing infinite dimensional system

implementation reveals limitations of finite dimensional, non-invariant design method - position and orientation don't work well together

shows that new research into invariant design is promising avenue of research, clear ways to solve problems encountered with this implementation

Bibliography

- [1] P. Stavroulakis and P. Sarachik, “Design of optimal controllers for distributed systems using finite dimensional state observers,” in *Decision and Control including the 12th Symposium on Adaptive Processes, 1973 IEEE Conference on.* IEEE, 1973, pp. 105–109.
- [2] L. Meirovitch and H. Baruh, “On the problem of observation spillover in self-adjoint distributed-parameter systems,” *Journal of Optimization Theory and Applications*, vol. 39, no. 2, pp. 269–291, 1983.
- [3] C. Harkort and J. Deutscher, “Finite-dimensional observer-based control of linear distributed parameter systems using cascaded output observers,” *International Journal of Control*, vol. 84, no. 1, pp. 107–122, 2011.
- [4] R. V. Gressang and G. B. Lamont, “Observers for systems characterized by semigroups,” *Automatic Control, IEEE Transactions on*, vol. 20, no. 4, pp. 523–528, 1975.
- [5] A. Smyshlyaev and M. Krstic, “Backstepping observers for a class of parabolic pdes,” *Systems & Control Letters*, vol. 54, no. 7, pp. 613–625, 2005.
- [6] K. Ramdani, M. Tucsnak, and G. Weiss, “Recovering the initial state of an infinite-dimensional system using observers,” *Automatica*, vol. 46, no. 10, pp. 1616–1625, 2010.
- [7] G. Haine, “Recovering the observable part of the initial data of an infinite-dimensional linear system with skew-adjoint generator,” *Mathematics of Control, Signals, and Systems*, vol. 26, no. 3, pp. 435–462, 2014.
- [8] J. Primbs, “Survey of nonlinear observer design techniques,” 1996.

- [9] C.-Z. Xu, P. Ligarius, and J.-P. Gauthier, “An observer for infinite-dimensional dissipative bilinear systems,” *Computers & Mathematics with Applications*, vol. 29, no. 7, pp. 13–21, 1995.
- [10] H. Bounit and H. Hammouri, “Observers for infinite dimensional bilinear systems,” *European journal of control*, vol. 3, no. 4, pp. 325–339, 1997.
- [11] S. I. Marcus, “Algebraic and geometric methods in nonlinear filtering,” *SIAM Journal on Control and Optimization*, vol. 22, no. 6, pp. 817–844, 1984.
- [12] S. Salcudean, “A globally convergent angular velocity observer for rigid body motion,” *Automatic Control, IEEE Transactions on*, vol. 36, no. 12, pp. 1493–1497, 1991.
- [13] N. Aghannan and P. Rouchon, “On invariant asymptotic observers,” in *Decision and Control, 2002, Proceedings of the 41st IEEE Conference on*, vol. 2. IEEE, 2002, pp. 1479–1484.
- [14] D. S. Maithripala, W. P. Dayawansa, and J. M. Berg, “Intrinsic observer-based stabilization for simple mechanical systems on lie groups,” *SIAM journal on control and optimization*, vol. 44, no. 5, pp. 1691–1711, 2005.
- [15] S. Bonnabel and P. Rouchon, “On invariant observers,” in *Control and observer design for nonlinear finite and infinite dimensional systems*. Springer, 2005, pp. 53–65.
- [16] S. Bonnabel, P. Martin, and P. Rouchon, “Symmetry-preserving observers,” *Automatic Control, IEEE Transactions on*, vol. 53, no. 11, pp. 2514–2526, 2008.
- [17] ——, “Non-linear symmetry-preserving observers on lie groups,” *Automatic Control, IEEE Transactions on*, vol. 54, no. 7, pp. 1709–1713, 2009.
- [18] D. Auroux and S. Bonnabel, “Symmetry-based observers for some water-tank problems,” *Automatic Control, IEEE Transactions on*, vol. 56, no. 5, pp. 1046–1058, 2011.
- [19] R. Mahony, T. Hamel, J. Trumpf, and C. Lageman, “Nonlinear attitude observers on so (3) for complementary and compatible measurements: A theoretical study,” in *Decision and Control, 2009 held jointly with the 2009 28th Chinese Control Conference. CDC/CCC 2009. Proceedings of the 48th IEEE Conference on*. IEEE, 2009, pp. 6407–6412.

- [20] J. Trumpf, R. Mahony, T. Hamel, and C. Lageman, “Analysis of non-linear attitude observers for time-varying reference measurements,” *Automatic Control, IEEE Transactions on*, vol. 57, no. 11, pp. 2789–2800, 2012.
- [21] R. Mahony, J. Trumpf, and T. Hamel, “Observers for kinematic systems with symmetry,” in *Proceedings of the 9th IFAC symposium on nonlinear control systems*, vol. 9, 2013, pp. 617–633.
- [22] N. Zarrouati-Vissière, “Augmented reality: the fusion of vision and navigation,” Ph.D. dissertation, Ecole Nationale Supérieure des Mines de Paris, 2013.
- [23] J. D. Adarve, D. J. Austin, and R. Mahony, “A filtering approach for computation of real-time dense optical-flow for robotic applications.”
- [24] C.-S. Park, D. Kim, B.-J. You, and S.-R. Oh, “Characterization of the hokuyo ubg-04lx-f01 2d laser rangefinder,” in *RO-MAN, 2010 IEEE*. IEEE, 2010, pp. 385–390.